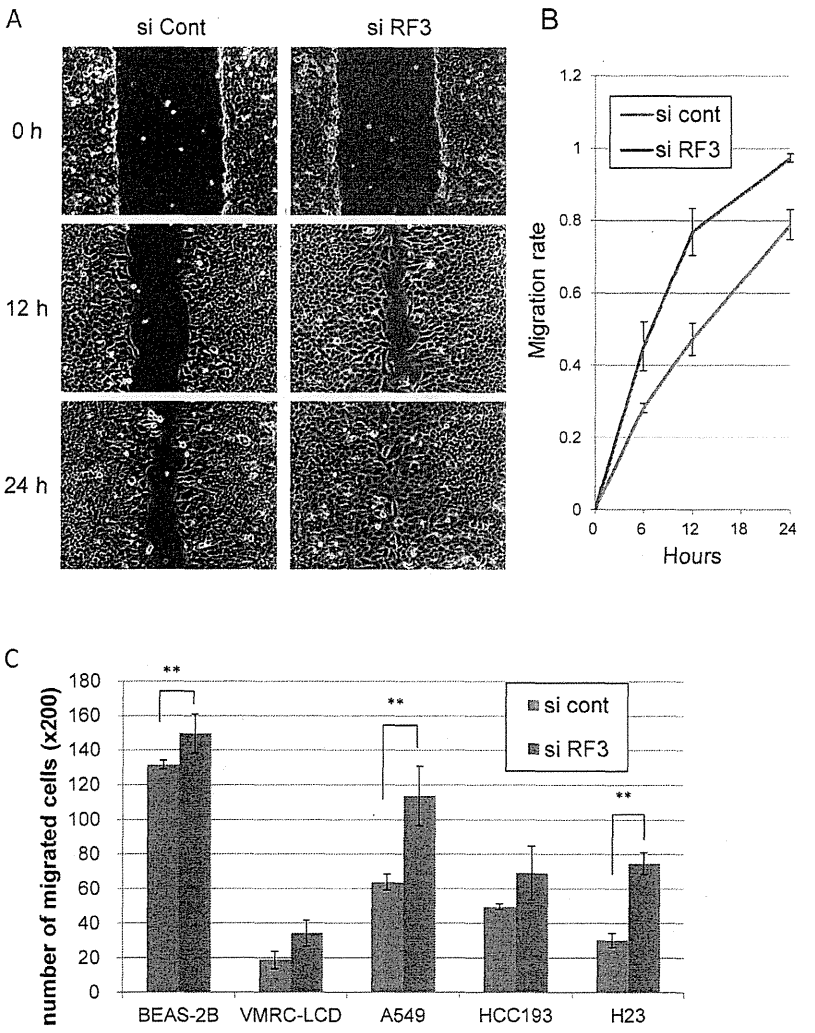


**Fig. 2.** RASSF3 knockdown enhances cell motility in the wound healing assay (A and B) and transwell migration assay (C). (A) Forty-eight hours after the transfection, A549 cells were re-plated in 3.5 cm dishes. After the cells had grown to confluence, cultures were damaged using 1–200 μl beveled orifice tip and then allowed to migrate. Photographs were taken at the indicated time points. (B) Migration rate is designated as a – b/a (a and b represent the widths of the fissures at time 0 and each time point, respectively). RASSF3-knockdown cells increased migration rate compared to the control. (C) Transwell migration assay. Cell lines transfected with siRNA were re-plated into a transwell chamber 48 h after the transfection and cells were counted after 24 h incubation. RASSF3-knockdown statistically significantly enhanced migration ability of 3 cell lines (A549, BEAS-2B, and NCI-H23). Although HCC193 also showed enhancement by RASSF3-knockdown, it was not statistically significant. The migration ability of VMRC-LCD was exceptionally low, and hardly affected by RASSF3-knockdown. *si RF3*: siRNA against RASSF3; *si Cont*: negative control siRNA.

### 3.4. DNA hypermethylation not a main cause of *RASSF3* downregulation

In order to determine whether or not low *RASSF3* expression was induced by DNA hypermethylation, we studied the DNA methylation status at the CpG island of the *RASSF3* gene promoter region using lung cancer cell lines. Fourteen lung cancer cell lines showed various *RASSF3* expression levels compared with an immortalized normal bronchial epithelial cell line BEAS-2B, the majority of which showed lower expression than in BEAS-2B (Supplemental Fig. 3A). However, we detected no CpG island methylation in the promoter region of the *RASSF3* gene in 14 lung cancer cell lines (Supplemental Fig. 3B). We also examined 8 NSCLC clinical samples from the low *RASSF3* expression group. However, we could not find DNA methylation in any specimens. These results suggested that DNA hypermethylation was not a major cause of *RASSF3* downregulation (Supplemental Fig. 3C).

### 3.5. Silence of *RASSF3* increases migration rate in NSCLC cells

The above results suggested that RASSF3 downregulation was associated with more malignant phenotypes including lymph node metastasis. To determine whether RASSF3 suppression promotes lung cancer cell migration ability in vitro, we transfected either RASSF3 targeted or control siRNA into four lung cancer cell lines (A549, HCC193, NCI-H23, and VMRC-LCD) and one immortalized bronchial epithelial cell line (BEAS-2B), and conducted wound healing and transwell migration assays. In the wound healing assay, migration ability was increased in RASSF3-knockdown A549 cells compared to the control cells (Fig. 2A and B). Similar results were obtained with three other cell lines including BEAS-2B, NCI-H23, and HCC193 (Supplemental Fig. S4). Similarly, in the transwell migration assay, RASSF3-knockdown enhanced migration ability of those 4 cell lines (A549, HCC193, NCI-H23, and BEAS-2B), although the enhancement in HCC193 was not statistically significant (Fig. 2C

and Supplemental Fig. S5). Because the migration ability of VMRC-LCD was exceptionally low, the effect of RASSF3-knockdown can be hardly evaluated in this cell line (Fig. 2C, Supplemental Figs. S4D, S4H, and S5).

## 4. Discussion

In the present study, we demonstrated that *RASSF3* expression was frequently downregulated in NSCLCs. Decrease of its expression was significantly associated with the progressive phenotypes of lung cancer including lymph node metastasis and pleural invasion. The strong correlation of lower *RASSF3* expression with such malignant phenotypes may imply that *RASSF3* downregulation plays an important role in cancer cell migration or invasion. This idea is supported by our in vitro studies which showed that RASSF3 knockdown promoted cell migration abilities of lung cancer cell lines. In this regard, we previously reported that RASSF3 stabilized p53 [16], and p53 was also shown to negatively regulate epithelial to mesenchymal transition (EMT) induced by TGF-β [20]. One possible mechanism of the tumor suppressive activity of RASSF3 might be a negative control of EMT through p53 stabilization. In this regard, EMT induction has been indicated to account for increased cancer cell migration/invasion [21]. However, although our preliminary in vitro experiments were suggestive, they failed to provide sufficient evidence to confirm EMT induction in the lung cancer cells by RASSF3-knockdown (data not shown).

The low *RASSF3* expression group also showed a correlation with wild-type *EGFR* status in univariate analysis. Multivariate analysis also revealed this correlation between RASSF3 and EGFR, indicating that this relationship was independent from other parameters. These data might suggest that the signaling pathways were regulated by RASSF3 and EGFR crosstalk in-between, and thus the alteration or mutation of each gene is mutually exclusive. On this point, Cui et al. reported that desmocollin 3, the target gene of p53, inhibits the EGFR/ERK pathway in human lung cancer [22]. Since RASSF3 stabilizes p53 [16], RASSF3 silencing might downregulate desmocollin 3 expression through p53 destabilization, resulting in activation of the EGFR/ERK pathway. However, further studies are needed to clarify whether or not such an interaction between the EGFR and RASSF3 signaling exists.

We found no significant correlation between *RASSF3* expression and patients' survival. This seemed to contradict the significant correlation of *RASSF3* with lymph node metastasis or pleural invasion in this study, where both were strong predictors of poor prognosis [23–25]. In this regard, previous studies reported that postoperative therapy has a strong influence on patients' survival, which we had earlier suspected to explain this inconsistency [26,27]. However, we found no remarkable difference in postoperative treatment between the two expression groups. Although we conducted further subset analyses of various kinds to explain this discrepancy, no significant factors were identified.

Finally, to determine the underlying mechanisms of *RASSF3* downregulation, we examined 14 lung cancer cell lines and 8 lung tumor specimens from the low expression group. However, we found no methylation of CpGs in the *RASSF3* promoter region. Previous studies also reported no methylation of *RASSF3* in 8 colorectal cancer cell lines, 8 thyroid cancer cell lines or 6 glioma cell lines [28–30]. Thus, simple hypermethylation of the promoter region may not be the primary mechanism to suppress RASSF3 transcription.

In conclusion, the present study showed that RASSF3 is frequently downregulated in NSCLCs, leading to an increase in lymph node metastasis or pleural invasion. These results indicate that RASSF3 is a tumor suppressor of lung cancer. Furthermore, the possible interaction between the RASSF3 and EGFR signaling might give new clues to dissect the complicated pathogenesis of lung cancer, which has long been virtually insurmountable riddle.

## Conflict of interest statement

None declared.

## Acknowledgments

This work was supported in part by JSPS KAKENHI (22300338, 2465065 YS, 23790725 KN, 22590267 YH), and a Grant-in-Aid for Third-Term Comprehensive Control Research for Cancer from the Ministry of Health, Labor and Welfare of Japan, and the Takeda Science Foundation (YS, KN). We thank Ms. Miwako Nishizawa for her excellent technical assistance.

## Appendix A. Supplementary data

Supplementary data associated with this article can be found, in the online version, at http://dx.doi.org/10.1016/j.lungcan.2013.10.014.

## References

[1] Jemal A, Bray F, Center MM, Ferlay J, Ward E, Forman D. Global cancer statistics. CA Cancer J Clin 2011;61:69–90.
[2] Richter AM, Pfeifer GP, Dammann RH. The RASSF proteins in cancer; from epigenetic silencing to functional characterization. Biochim Biophys Acta 2009;1796:114–28.
[3] Pfeifer GP, Dammann R, Tommasi S. RASSF proteins. Curr Biol 2010;20:R344–5.
[4] Sherwood V, Recino A, Jeffries A, Ward A, Chalmers AD. The N-terminal RASSF family: a new group of Ras-association-domain-containing proteins, with emerging links to cancer formation. Biochem J 2010;425:303–11.
[5] Underhill-Day N, Hill V, Latif F. N-terminal RASSF family: RASSF7-RASSF10. Epigenetics 2011;6:284–92.
[6] Dammann R, Li C, Yoon JH, Chin PL, Bates S, Pfeifer GP. Epigenetic inactivation of a RAS association domain family protein from the lung tumour suppressor locus 3p21.3. Nat Genet 2000;25:315–9.
[7] Burbee DG, Forgacs E, Zochbauer-Muller S, Shivakumar L, Fong K, Gao B, et al. Epigenetic inactivation of RASSF1A in lung and breast cancers and malignant phenotype suppression. J Natl Cancer Inst 2001;93:691–9.
[8] Endoh H, Yatabe Y, Shimizu S, Tajima K, Kuwano H, Takahashi T, et al. RASSF1A gene inactivation in non-small cell lung cancer and its clinical implication. Int J Cancer 2003;106:45–51.
[9] Ito M, Ito G, Kondo M, Uchiyama M, Fukui T, Mori S, et al. Frequent inactivation of RASSF1A, BLU, and SEMA3B on 3p21.3 by promoter hypermethylation and allele loss in non-small cell lung cancer. Cancer Lett 2005;225:131–9.
[10] Wang J, Wang B, Chen X, Bi J. The prognostic value of RASSF1A promoter hypermethylation in non-small cell lung carcinoma: a systematic review and meta-analysis. Carcinogenesis 2011;32:411–6.
[11] Jo H, Kim JW, Kang GH, Park NH, Song YS, Kang SB, et al. Association of promoter hypermethylation of the RASSF1A gene with prognostic parameters in endometrial cancer. Oncol Res 2006;16:205–9.
[12] Ma L, Zhang JH, Liu FR, Zhang X. Hypermethylation of promoter region of RASSF1A gene in ovarian malignant epithelial tumors. Zhonghua Zhong Liu Za Zhi 2005;27:657–9.
[13] Sugawara W, Haruta M, Sasaki F, Watanabe N, Tsunematsu Y, Kikuta A, et al. Promoter hypermethylation of the RASSF1A gene predicts the poor outcome of patients with hepatoblastoma. Pediatr Blood Cancer 2007;49:240–9.
[14] Tommasi S, Dammann R, Jin SG, Zhang XF, Avruch J, Pfeifer GP. RASSF3 and NORE1: identification and cloning of two human homologues of the putative tumor suppressor gene RASSF1. Oncogene 2002;21:2713–20.
[15] Jacquemart IC, Springs AE, Chen WY. Rassf3 is responsible in part for resistance to mammary tumor development in neu transgenic mice. Int J Oncol 2009;34:517–28.
[16] Kudo T, Ikeda M, Nishikawa M, Yang Z, Ohno K, Nakagawa K, et al. The RASSF3 candidate tumor suppressor induces apoptosis and G1-S cell-cycle arrest via p53. Cancer Res 2012;72:2901–11.
[17] Paez JG, Janne PA, Lee JC, Tracy S, Greulich H, Gabriel S, et al. EGFR mutations in lung cancer: correlation with clinical response to gefitinib therapy. Science 2004;304:1497–500.
[18] Pao W, Miller V, Zakowski M, Doherty J, Politi K, Sarkaria I, et al. EGF receptor gene mutations are common in lung cancers from never smokers and are associated with sensitivity of tumors to gefitinib and erlotinib. Proc Natl Acad Sci U S A 2004;101:13306–11.
[19] Shigematsu H, Lin L, Takahashi T, Nomura M, Suzuki M, Wistuba II, et al. Clinical and biological features associated with epidermal growth factor receptor gene mutations in lung cancers. J Natl Cancer Inst 2005;97:339–46.

[20] Termen S, Tan EJ, Heldin CH, Moustakas A. p53 regulates epithelial-mesenchymal transition induced by transforming growth factor beta. J Cell Physiol 2013;228:801–13.
[21] Thomson S, Petti F, Sujka-Kwok I, Mercado P, Bean J, Monaghan M, et al. A systems view of epithelial-mesenchymal transition signaling states. Clin Exp Metastasis 2011;28:137–55.
[22] Cui T, Chen Y, Yang L, Knosel T, Huber O, Pacyna-Gengelbach M, et al. The p53 target gene desmocollin 3 acts as a novel tumor suppressor through inhibiting EGFR/ERK pathway in human lung cancer. Carcinogenesis 2012;33:2326–33.
[23] Fukui T, Mori S, Yokoi K, Mitsudomi T. Significance of the number of positive lymph nodes in resected non-small cell lung cancer. J Thorac Oncol 2006;1:120–5.
[24] Shimizu K, Yoshida J, Nagai K, Nishimura M, Ishii G, Morishita Y, et al. Visceral pleural invasion is an invasive and aggressive indicator of non-small cell lung cancer. J Thorac Cardiovasc Surg 2005;130:160–5.
[25] Kanzaki R, Ikeda N, Okura E, Kitahara N, Shintani Y, Okimura A, et al. Surgical results and staging of non-small cell lung cancer with interlobar pleural invasion. Interact Cardiovasc Thorac Surg 2012;14:739–42.
[26] Heon S, Johnson BE. Adjuvant chemotherapy for surgically resected non-small cell lung cancer. J Thorac Cardiovasc Surg 2012;144: S39–42.
[27] Tsuboi M, Ohira T, Saji H, Miyajima K, Kajiwara N, Uchida O, et al. The present status of postoperative adjuvant chemotherapy for completely resected non-small cell lung cancer. Ann Thorac Cardiovasc Surg 2007;13: 73–7.
[28] Hesson LB, Wilson R, Morton D, Adams C, Walker M, Maher ER, et al. CpG island promoter hypermethylation of a novel Ras-effector gene RASSF2A is an early event in colon carcinogenesis and correlates inversely with K-ras mutations. Oncogene 2005;24:3987–94.
[29] Schagdarsurengin U, Richter AM, Hornung J, Lange C, Steinmann K, Dammann RH. Frequent epigenetic inactivation of RASSF2 in thyroid cancer and functional consequences. Mol Cancer 2010;9:264.
[30] Hesson L, Bieche I, Krex D, Criniere E, Hoang-Xuan K, Maher ER, et al. Frequent epigenetic inactivation of RASSF1A and BLU genes located within the critical 3p21.3 region in gliomas. Oncogene 2004;23:2408–19.

Cancer Chemother Pharmacol (2013) 72:1063–1071
DOI 10.1007/s00280-013-2277-8

ORIGINAL ARTICLE

# A phase I, pharmacokinetic and pharmacodynamic study of nimotuzumab in Japanese patients with advanced solid tumors

**Wataru Okamoto · Takayuki Yoshino · Toshiaki Takahashi · Isamu Okamoto · Shinya Ueda · Asuka Tsuya · Narikazu Boku · Kazuto Nishio · Masahiro Fukuoka · Nobuyuki Yamamoto · Kazuhiko Nakagawa**

Received: 25 October 2012 / Accepted: 21 August 2013 / Published online: 18 September 2013


**Abstract**
*Purpose* Nimotuzumab is a humanized $IgG_1$ monoclonal antibody to the epidermal growth factor receptor (EGFR) and has demonstrated the absence of severe dermatological toxicity commonly caused by other EGFR-targeting antibodies. We conducted a phase I study to assess toxicities, pharmacokinetics, pharmacodynamics, and predictive biomarkers of nimotuzumab administered in Japanese patients with advanced solid tumors.
*Methods* Three dose levels, 100, 200, and 400 mg, of weekly i.v. nimotuzumab were given until disease progression or drug intolerability. Four patients with solid tumors were enrolled in each dose level. The expression and gene copy number of *EGFR* or its downstream transducers were investigated using skin biopsy samples and tumor specimens.
*Results* Planned dose escalation was completed without dose-limiting toxicity, and maximum tolerated dose was not reached. No allergic reaction and hypomagnesaemia were observed, and grade 3 or 4 toxicity did not occur. The common toxicity was skin rash (58 %); however, all of them were grade 1 or 2. In skin biopsies, no correlation was shown between doses and the phosphorylation of EGFR or its downstream signal transducers. Of 11 evaluable patients, no objective response was obtained, while 8 patients had stable disease (73 %). Patients with a higher-*EGFR* gene copy number level measured by FISH showed a longer time to progression.
*Conclusions* Nimotuzumab administered weekly was feasible and well tolerated up to 400 mg in Japanese patients. A low dermatological toxicity could be a notable advantage as anti-EGFR mAb, and further evaluation is warranted.

**Keywords** Nimotuzumab · EGFR · Phase 1 · Pharmacokinetics · Solid tumor

**Electronic supplementary material** The online version of this article (doi:10.1007/s00280-013-2277-8) contains supplementary material, which is available to authorized users.

W. Okamoto (✉) · I. Okamoto · S. Ueda · M. Fukuoka · K. Nakagawa
Department of Medical Oncology, Kinki University Faculty of Medicine, 377-2 Ohno-Higashi, Osaka-Sayama, Osaka 589-8511, Japan
e-mail: wataru_okamoto@dotd.med.kindai.ac.jp

T. Yoshino · N. Boku
Division of Gastrointestinal Oncology, Shizuoka Cancer Center, 1007 Shimonagakubo, Nagaizumi-cho, Sunto-gun, Shizuoka 411-8777, Japan

T. Takahashi · A. Tsuya · N. Yamamoto
Division of Thoracic Oncology, Shizuoka Cancer Center, 1007 Shimonagakubo, Nagaizumi-cho, Sunto-gun, Shizuoka 411-8777, Japan

K. Nishio
Department of Genome Biology, Kinki University Faculty of Medicine, 377-2 Ohno-Higashi, Osaka-Sayama, Osaka 589-8511, Japan

## Introduction

Epidermal growth factor receptor (EGFR) has become one of the most widely explored targets for anticancer therapy, because EGFR overexpression is implicated in tumor cell proliferation, invasion, angiogenesis, and metastasis [1, 2].

Several EGFR antagonists including monoclonal antibodies and small tyrosine kinase inhibitors have been investigated in colorectal cancer, head and neck cancer, and non-small cell lung cancer. However, these agents also

act on normal human epithelial cells with a comparatively higher appearance of EGFR. As a result, dermatological toxicity including acneiform skin rash could compromise patient's quality of life (QOL) and worsen the compliance of treatment [3–5].

Nimotuzumab is a recombinant humanized monoclonal antibody against human EGFR, which is a human $IgG_1$. It has demonstrated blocking ability against the binding of EGF and TGF-alpha to EGFR, and also cytotoxic activity through antibody-dependent cellular cytotoxicity (ADCC) and complement-dependent cytotoxicity (CDC). In non-clinical studies, inhibition activity on tumor cell growth, angiogenesis, and apoptosis has been observed [6–8]. Nimotuzumab has shown clinical efficacy in head and neck cancer or glioma as combination therapy with radiotherapy [9–13]. In these clinical studies, nimotuzumab has demonstrated low frequency or absence of severe dermatological toxicity. This unique safety profile could be expected to contribute to the better QOL for patients.

The reason for low frequency of dermatological toxicity has been investigated in several recent researches [14, 15]. According to the findings, the possible explanation of low frequency of dermatological toxicity is regarded as (1) its intermediate affinity ($Kd = 10^{-8}$ M), which is at least one order lower magnitude than cetuximab or panitumumab, and (2) the difference in binding profile, where nimotuzumab requires bivalent binding for stable attachment to the cellular surface in contrast to cetuximab requiring only monovalent binding. Due to these properties, nimotuzumab could attach to EGFR only when the EGFR surface density is high enough to allow bivalent binding. EGFR is commonly overexpressed on tumor cells compared with the expression levels on normal cells; consequently, nimotuzumab could selectively attach to tumor cells without binding to normal cells.

In a previous phase I study in Canada, the tolerability of nimotuzumab was investigated up to 800 mg dose per week and did not reach MTD though one DLT was observed in the 100 mg group [16]. Subsequently, several trials demonstrated the efficacy of nimotuzumab administered 200 mg weekly to the patients with head and neck squamous cell cancer, glioma, and non-small cell lung cancer. The dose in clinical use has been set as 200 mg per week in combination with radiotherapy in several countries. According to the clinical dose in other countries, we evaluated the safety and pharmacokinetics profile of nimotuzumab at the dose levels of 100, 200, and 400 mg weekly in Japanese patients with advanced solid tumors. The secondary objectives were to assess tumor response, pharmacodynamic (PD) effects using skin tissue, and biomarkers to predict the clinical efficacy of nimotuzumab.

## Methods

### Patient eligibility

Patients with histologically or cytologically confirmed advanced solid tumors either refractory to standard therapy or for which no effective standard treatment existed were eligible if they fulfilled all of the following criteria: age between 20 and 75 years; ECOG performance status (PS) of 0–1; life expectancy of $\geq$3 months; adequate bone marrow, liver, and renal functions; and arterial oxygen pressure ($PaO_2$) $\geq$70 mmHg. Exclusion criteria included previous exposure to EGFR-targeted antibodies; brain metastases that required systemic medication; obvious pneumonitis or pulmonary fibrosis confirmed by chest CT (computed tomography).

The protocol was approved by the independent ethical committee at each center and carried out according to the principles of the Declaration of Helsinki and Good Clinical Practice guidelines. All patients gave written informed consent before study entry.

Written informed consent for the pharmacodynamics and biomarker analysis was additionally obtained from those who submitted their tumor and skin biopsy samples.

### Screening and study assessments

Physical examination, radiographic tumor assessment, ECG, and chest CT investigation were performed within 28 days prior to the first dose of nimotuzumab. A pregnancy test was checked from women with childbearing potential.

Nimotuzumab was administered intravenously every week over 30 min without pre-medication for preventing allergic reaction. Each cycle was defined as 4 weeks, and treatment was continued until disease progression, occurrence of intolerable toxicity, or patient's withdrawal of consent.

Before each cycle, physical examination including vital signs, ECOG PS, blood tests including complete blood cell count and biochemistry including KL-6 were conducted. Toxicities were assessed according to the National Cancer Institute Common Terminology Criteria for Adverse Events (CTCAE) version 3.0. Tumor response was assessed after 4 weeks, thereafter at least every 8 weeks using Response Evaluation Criteria in Solid Tumors (RECIST) criteria version 1.0.

### Treatment administration and dose escalation procedure

The initial dose of nimotuzumab was 100 mg, and the dose was escalated to 200 and 400 mg.

DLTs were initially evaluated in at least 3 patients for each dose level, and the escalation to the next dose level was implemented if less than 1/3 of the patients experienced

DLT. When one patient experienced a DLT, additional three patients were enrolled and the incidence of DLTs was evaluated in a total of six evaluable patients at each level. DLTs were defined as the following toxicities related to nimotuzumab: (1) CTCAE grade 4 fatigue, hematotoxicity, nausea, vomiting, diarrhea, or electrolyte abnormality; (2) grade 3 nausea, vomiting, or diarrhea persisting despite administration of maximum supportive care; (3) grade 3 or higher fatigue persisting for 7 days or longer; (4) any toxicity causing postponement of treatment continuously twice. DLTs were assessed during the first cycle at each dose level. The MTD was defined as the lowest dose at which 33 % or more of patients experienced DLT in the first cycle.

### Pharmacokinetic analysis

Blood samples (3 mL) were collected prior to the first dosing and at 5 min, 1, 3, 8, 24, 48, and 72 h after dosing on day 1, and prior to and 5 min after dosing on days 8, 15, 22, 29, 36, and 50. Serum concentration of nimotuzumab was analyzed using the ELISA method as shown in the Online Resource 1. The lower detection limit for the serum concentration of nimotuzumab was 2 μg/mL. The pharmacokinetic (PK) parameters in the first cycle were calculated by a non-compartment analysis using the computer software SAS version 8.2 (SAS Institute, Japan) with the same analytical approach as the bolus model generated by WinNonlin Professional (5.2.1, Pharsight, Mountain View, California). The maximum concentration ($C_{max}$) and time to $C_{max}$ ($t_{max}$) were obtained by measured values. The apparent elimination half-life ($t_{1/2}$) was obtained by linear regression of 3 or more log-transformed data points in the terminal phase. The area under the concentration versus the time curve up to the time of the last measurable concentration data ($AUC_{0-168h}$) was obtained by the trapezoidal method (linear up/log down). The AUC values were extrapolated to infinity ($AUC_{0-inf}$) using the equation $AUC_{0-168h} + C_{168h}/\lambda$, where $C_{168h}$ is the last measurable concentration, and $\lambda$ is the terminal elimination rate. The total body clearances ($CL_t$) were calculated by the equation $Dose/AUC_{0-inf}$.

### Immunogenicity (human anti-humanized antibody)

Serum samples for the analysis on human anti-humanized antibody (HAHA) were collected prior to the first administration and at the end of the first cycle and repeated at least once every 2 cycles. HAHA was measured by the ELISA method as shown in the Online Resource 2.

### Pharmacodynamic analysis using skin tissue samples

Skin biopsy was performed prior to the first administration and after fifth administration on patients who provided consent for participating in the PD analysis. Expression status of EGFR, phosphorylated EGFR (p-EGFR), AKT, phosphorylated AKT (p-AKT), MAPK, phosphorylated MAPK (p-MAPK), and Ki-67 in the skin samples were analyzed by the immunohistochemical staining. EGFR PharmDx kit (Dako, Glostrup, Denmark) was used for detection of EGFR. p-EGFR, AKT, p-AKT, MAPK, p-MAPK, and Ki-67 were detected by the primary antibodies of phospho-EGFR (Y1068) Rabbit mAb (EP774Y) (abcam), AKT1 rabbit mAb #4685 (Cell signaling, Beverly, MA, USA), phospho-AKT (Ser 473) rabbit mAb #3787 (Cell signaling), p44/42 MAP Kinase Ab #9102, phospho-p44/42 MAP Kinase (Thr202/Tyr204) Rabbit mAb #4376 (Cell signaling), and Ki-67 Ab #M7240 (Dako, Glostrup, Denmark), respectively. Protein expression levels were evaluated as positive cell rates (%) calculated by the number of positive cells per 100 cells under microscope.

### Biomarker research using tumor tissue samples

Immunohistochemical staining for EGFR and its downstream signal transducers was performed with paraffin-embedded sections of tumor samples. The antibodies used for tumor tissue samples were the same as those in the PD analysis using skin biopsies. The positive cell rate (%) was calculated based on the number of positive cells per 100 tumor cells under microscope.

*EGFR* gene status was investigated by FISH, Paraffin pretreatment kit, LSI EGFR SpectrumOrange/CEP7 SpectrumGreen probe, DAPI I (Vysis, USA), and IGEPAL CA-630 (Sigma, USA). The numbers of *EGFR* gene and chromosome 7 centromeres were counted in 20 tumor cells and assessed for amplification or aneuploidy. Patients were classified into six FISH strata: (1) disomy (≤2 copies in >90 % of cells); (2) low trisomy (3 copies in 10–39 % of the cells); (3) high trisomy (3 copies in ≥40 % of cells); (4) low polysomy (≥4 copies in 10–39 % of cells); (5) high polysomy (≥4 copies in ≥40 % of cells); and (6) gene amplification (defined by presence of tight *EGFR* gene clusters and a ratio of *EGFR* gene to chromosome 7 centromere of ≥2 or ≥15 copies of *EGFR* per cell in ≥10 % of analyzed cells) [18, 19].

## Results

### Patient characteristics

From May 22, 2007, to August 1, 2008, 13 patients were enrolled in this study; however, one patient with colorectal cancer registered to the 100 mg dose level withdrew from the study before administration of nimotuzumab in order to receive radiation therapy for bone metastasis. Four patients were administered nimotuzumab at each level and included

in the safety analysis population and the MTD analysis population. Their characteristics are shown in Table 1. Of these 12 patients, the tumor types were 5 colorectal cancer, 3 non-small cell lung cancer, 2 gastric cancer, 1 renal cancer, and 1 leiomyosarcoma. All patients had received previous chemotherapy regimens, and 8 of 12 patients had received more than 4 prior regimens. Of these 12 patients, 1 patient at the 100 mg level was judged as ineligible since there had been pleural effusion requiring drainage before enrollment. Therefore, that patient was excluded from the PK analysis population and efficacy analysis population.

**Table 1** Patient characteristics in safety analysis population

| Dose | 100 mg | 200 mg | 400 mg | All dose (%) |
|---|---|---|---|---|
| No. of treated patients | 4 | 4 | 4 | 12 |
| Age (years) | | | | |
| Mean ± SD | 53.0 ± 3.4 | 61.8 ± 9.4 | 56.8 ± 5.4 | 57.2 ± 7.0 |
| Sex | | | | |
| Female | 1 | 2 | 4 | 7 (58.3 %) |
| Male | 3 | 2 | 0 | 5 (41.7 %) |
| PS (ECOG) | | | | |
| 0 | 2 | 2 | 2 | 6 (50.0 %) |
| 1 | 2 | 2 | 2 | 6 (50.0 %) |
| No. of prior regimen | | | | |
| 1 | 1 | 0 | 1 | 2 (16.7 %) |
| 2 | 0 | 0 | 1 | 1 (8.3 %) |
| 3 | 1 | 0 | 0 | 1 (8.3 %) |
| ≥4 | 2 | 4 | 2 | 8 (66.7 %) |
| Primary tumor | | | | |
| Colorectal cancer | 2 | 2 | 1 | 5 (41.7 %) |
| NSCLC | 1 | 1 | 1 | 3 (25.0 %) |
| Gastric cancer | 0 | 1 | 1 | 2 (16.7 %) |
| Renal cancer | 0 | 0 | 1 | 1 (8.3 %) |
| Leiomyosarcoma | 1 | 0 | 0 | 1 (8.3 %) |

## Safety

Twelve patients had received a total of 52 cycles. The mean number of cycles was 4.3 (5.3, 2.8, and 5.0 at the dose levels of 100, 200, and 400 mg, respectively). The mean treatment period (± standard deviation) was 121.9 (± 77.5) days {147.5 (± 98.7), 79.0 (± 16.7), and 139.3 (± 90.8) days at the dose levels of 100, 200, and 400 mg, respectively}. All 12 patients discontinued nimotuzumab due to disease progression.

Table 2 presents the nimotuzumab-related adverse event during all cycles. No DLT was observed at any dose levels; therefore, the MTD was not reached up to 400 mg dose level. The most common adverse drug reaction observed in ≥15 % of patients were rash (50.0 %), anorexia (16.7 %), nausea (16.7 %), fatigue (16.7 %), aspartate aminotransferase increased (16.7 %), and blood alkaline phosphatase increased (16.7 %). As to dermatological toxicity, known as a class effect of anti-EGFR mAbs, one patient developed a grade 2 rash, whereas the other five patients of rash and one patient of dermatitis acneiform were of grade 1. No grade 3 or higher adverse drug reaction and no infusion reaction were observed at any dose levels, and there was no adverse drug reaction that led to a delay in treatment or dose reduction.

## Efficacy

Eleven patients were evaluable for anti-tumor response. While complete response and partial response were not achieved in any dose levels, stable disease was observed in 8 patients (72.7 %). Median time to progression (TTP) was 97 days in eleven patients.

## Pharmacokinetic analysis

Serum samples were evaluated for 11 patients. The mean serum concentration–time profile of nimotuzumab after the first administration in the first cycle is described in Fig. 1, and the PK profile of nimotuzumab is summarized in Table 3 and Fig. 2.

The serum nimotuzumab concentration after the first treatment on the first cycle reached maximum immediately after the infusion at all doses and decreased subsequently. The mean $t_{1/2}$ was 34, 47, and 75 h at a dose of 100, 200, and 400 mg, respectively.

$C_{max}$ and $AUC_{0-inf}$ of nimotuzumab increased in an exponential manner in the range of 100–400 mg. The mean total body clearances ($CL_t$) were 78.753, 47.358, and 28.960 mL/h at a dose of 100, 200 and 400 mg, respectively. The $CL_t$ showed exponential decrease from 100 to 400 mg, and the slope of $CL_t$ was gradual especially between 200 and 400 mg, similar to the previous PK study [17].

The serum concentration–time profile of nimotuzumab following the first administration in cycle 1 up to the fourth administration in cycle 2 is shown in Fig. 3.

Serum concentrations of nimotuzumab at each dose level increased along with the first and fourth administration and then reached plateau concentration by the fourth administration in cycle 2.

## HAHA response

The serum samples were collected from 12 patients at pre-treatment, cycle 1, 3, 5, 7, and 9 as possible. Totally 43 serum samples including 12 pre-treatment and 31 on-treatment samples were measured for HAHA. However, no HAHA was detected during the treatment cycles of all patients.

**Table 2** Adverse drug reaction during all cycles

| Event | 100 mg ($n = 4$) | | | 200 mg ($n = 4$) | | | 400 mg ($n = 4$) | | | All doses ($n = 12$) | |
|---|---|---|---|---|---|---|---|---|---|---|---|
| | Grade | | | Grade | | | Grade | | | | |
| | 1 | 2 | 3 | 1 | 2 | 3 | 1 | 2 | 3 | *n* | (%) |
| Non-hematologic toxicity | | | | | | | | | | | |
| Rash | 1 | 1 | | 2 | | | 2 | | | 6 | 50.0 |
| Nausea | | | | 1 | | | 1 | | | 2 | 16.7 |
| Fatigue | 1 | | | | | | 1 | | | 2 | 16.7 |
| Anorexia | | | | | 1 | | 1 | | | 2 | 16.7 |
| Bradycardia | | | | | | | 1 | | | 1 | 8.3 |
| Constipation | | | | | | | 1 | | | 1 | 8.3 |
| Diarrhea | 1 | | | | | | | | | 1 | 8.3 |
| Dyspepsia | | | | | | | 1 | | | 1 | 8.3 |
| Dermatitis acneiform | | | | | | | 1 | | | 1 | 8.3 |
| Hypothermia | | 1 | | | | | | | | 1 | 8.3 |
| Hematologic toxicity | | | | | | | | | | | |
| AST increased | | | | 1 | | | 1 | | | 2 | 16.7 |
| ALP increased | | | | 1 | | | | 1 | | 2 | 16.7 |
| ALT increased | | | | 1 | | | | | | 1 | 8.3 |
| γ-GTP increased | | | | | 1 | | | | | 1 | 8.3 |
| Albumin increased | | | | | | | 1 | | | 1 | 8.3 |
| Creatinine increased | | | | 1 | | | | | | 1 | 8.3 |
| Potassium increased | | | | 1 | | | | | | 1 | 8.3 |
| WBC count decreased | | | | | | | | 1 | | 1 | 8.3 |
| Neutrophil count decreased | | | | | | | | 1 | | 1 | 8.3 |

Adverse drug reaction was defined as those toxicities with 'definite', 'probable', 'possible' relativity to nimotuzumab, or 'unknown'

ALT: L-alanine aminotransferase, AST: L-aspartate aminotransferase, ALP: alkaline phosphatase, γ-GTP: γ-glutamyl transpeptidase, WBC: White blood cell

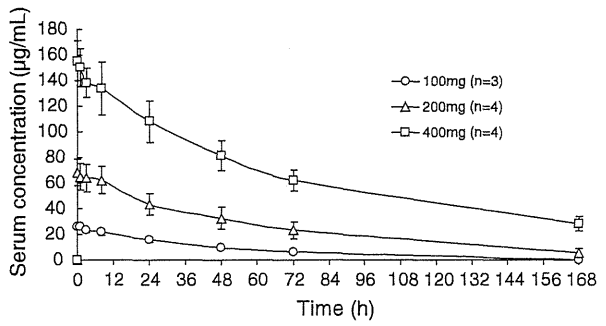


**Fig. 1** Serum concentration–time profile of nimotuzumab after the first administration in cycle 1. The arithmetic mean ± arithmetic SD of each time point for each group is shown

## Pharmacodynamic analysis using skin tissue

Skin samples at pre- and on-treatment were evaluated for 11 patients. The expression level of EGFR, p-EGFR, AKT, p-AKT, MAPK, p-MAPK, and Ki-67 was analyzed by immunohistochemical staining, and its positive cell rate was counted. However, these expression levels showed no certain tendency through pre- and on-treatment as shown in the table (Online Resource 3). Furthermore, no correlation was shown between the nimotuzumab doses and phosphorylation of EGFR, AKT, and MAPK.

## Correlation between the markers in tumor tissue and efficacy

In order to investigate the correlation between the biomarkers and nimotuzumab efficacy, tumor tissue was obtained from 8 patients, 2, 2, and 4 patients in 100, 200, and 400 mg dose level, respectively.

The gene copy number was determined by FISH and classified into 3 categories (−; disomy, low trisomy, and high trisomy, +; low polysomy, ++; high polysomy and gene amplification). The time to progression by *EGFR* gene copy number level was shown in Fig. 4. A tendency of longer TTP was observed in patients with higher-*EGFR* gene copy number level, though the sample size was limited and the tumor type was disparate in this study.

The levels of EGFR, AKT, p-AKT, MAPK, and p-MAPK detected by immunohistochemistry (IHC) showed no relationship with clinical efficacy as shown in the table (Online Resource 4).

**Table 3** Pharmacokinetic parameters after the first administration in cycle 1

| Pharmacokinetic parameter | Dose | | |
|---|---|---|---|
| | 100 mg | 200 mg | 400 mg |
| | $n = 3$ | $n = 4$ | $n = 4$ |
| $C_{max}$ (μg/mL) | 26.767 ± 1.026 | 68.550 ± 10.345 | 157.250 ± 15.064 |
| $t_{max}$ (h) | 0.687 ± 0.535 | 0.050 ± 0.029 | 0.540 ± 0.526 |
| $AUC_{0\text{-inf}}$ (μg h/mL) | 1,271.923 ± 63.245 | 4,521.940 ± 1,181.627 | 14,107.898 ± 2,342.115 |
| $CL_t$ (mL/h) | 78.753 ± 3.993 | 47.358 ± 16.074 | 28.960 ± 4.924 |
| $t_{1/2}$ (h) | 34.347 ± 3.332 | 47.498 ± 9.376 | 75.805 ± 6.986 |

Arithmetic mean ± arithmetic SD

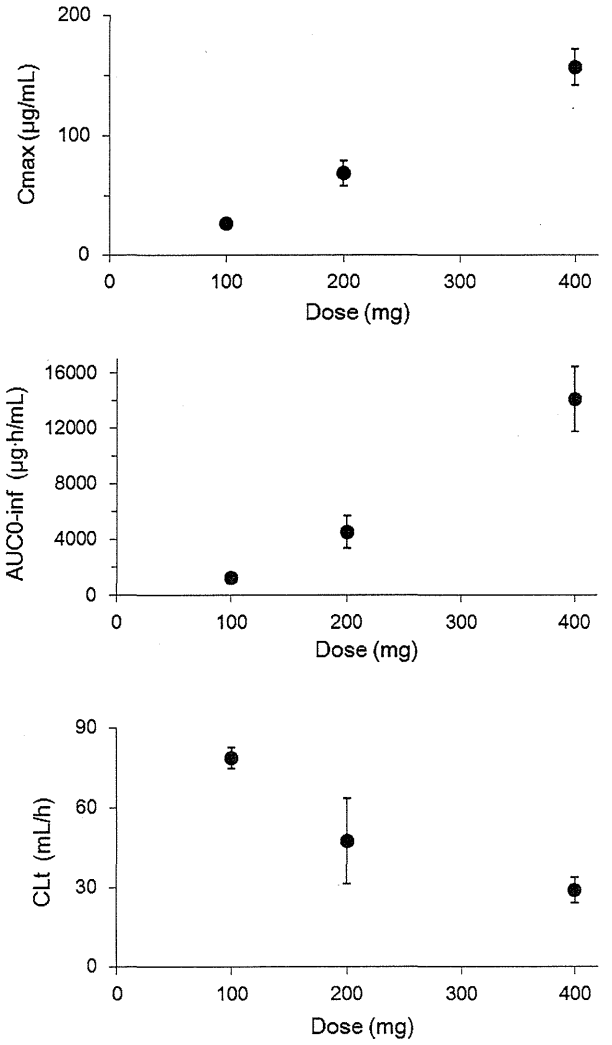


**Fig. 2** Dose relationship of $C_{max}$, $AUC_{0\text{-inf}}$, and $CL_t$ of nimotuzumab during the first administration in cycle 1. The arithmetic mean ± arithmetic SD 100 mg, $n = 3$; 200 mg, $n = 4$; 400 mg, $n = 4$

## Discussion

This is the first study on Japanese patients with solid tumors to investigate the safety and pharmacokinetics of 100, 200, and 400 mg nimotuzumab administered weekly. All 12 patients tolerated well the treatment of nimotuzumab at a dose of 100, 200, and 400 mg, without grade 3 or higher adverse events that led to treatment delay or dose reduction. No DLT was observed in the planned dose range of 100–400 mg nimotuzumab, and MTD was not reached. Furthermore, frequencies of adverse events did not increase with higher doses of nimotuzumab as the previous phase I study conducted in Canada [16]. These results suggest the absence of a dose-dependent toxicity relationship for nimotuzumab.

In this study, there is no grade 3 or 4 dermatological toxicity, and most of the dermatological toxicity was grade 1. The incidence of rash of all grades was 50 % in each dose level, however, localized to the limited body surface, and all of them were resolved during study treatment within approximately 1 week. Consistent with our study, nimotuzumab was previously reported to cause rarely severe skin toxicity [17, 26]; however, such toxicity is commonly observed in the clinical use of other anti-EGFR mAbs, leading to increase in patient risk for infections and early termination of the treatment [4, 5]. Furthermore, we demonstrated that no hypomagnesaemia was observed, similar to other nimotuzumab phase I studies [16]. Hypomagnesaemia is known as a common adverse event with other anti-EGFR mAbs as well as platinum-based chemotherapy and considered to be related to nephrotoxicity or cardiovascular toxicity [21–23]. Taken together, the safety profile of nimotuzumab could be expected to maintain good QOL as well as compliance and shows a potential to combine nimotuzumab with other drugs which cause dermatological toxicity or hypomagnesaemia.

In PK analysis, the trough concentration of nimotuzumab reached a steady state after the fourth cycle. The trough level was approximately 15 and 55 μg/mL in 200 and 400 mg, respectively, which reached the concentration to show the cell-growth inhibitory activity in the previous in vitro study [24]. The mean $t_{1/2}$ was approximately 34, 47, and 75 h at a dose of 100, 200, and 400 mg, respectively. Nimotuzumab is a humanized mAb; however, the $t_{1/2}$ was similar to cetuximab which is a chimeric antibody to EGFR, rather than the other humanized antibody such as

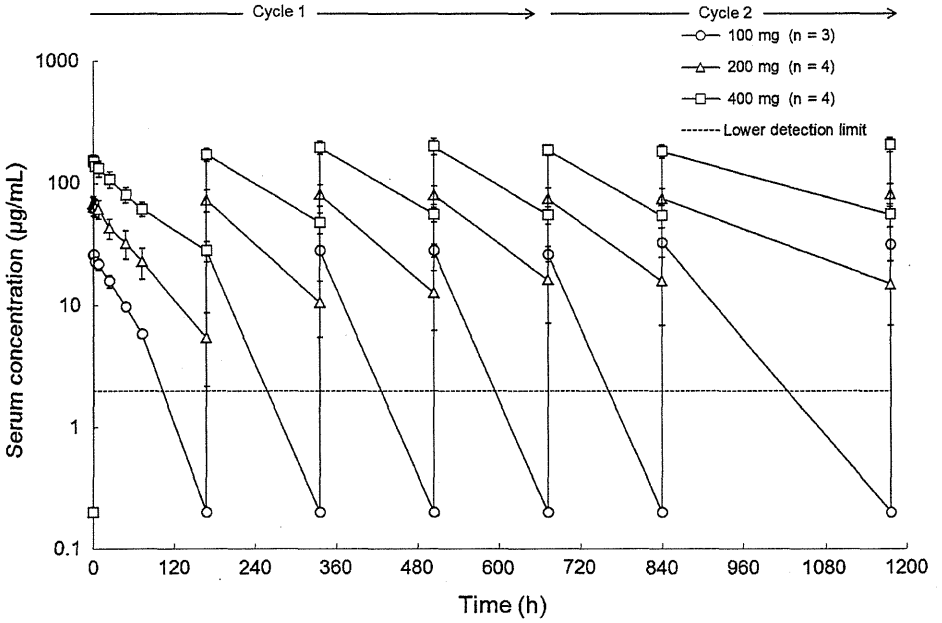


**Fig. 3** Serum concentration–time profile of nimotuzumab following the first administration in cycle 1 up to the fourth administration in cycle 2. The lower detection limit for the serum concentration was 2.00 (μg/mL). If the concentration was lower than 2.00 (μg/mL), the mark was set at 0.2 (μg/mL) in the figure

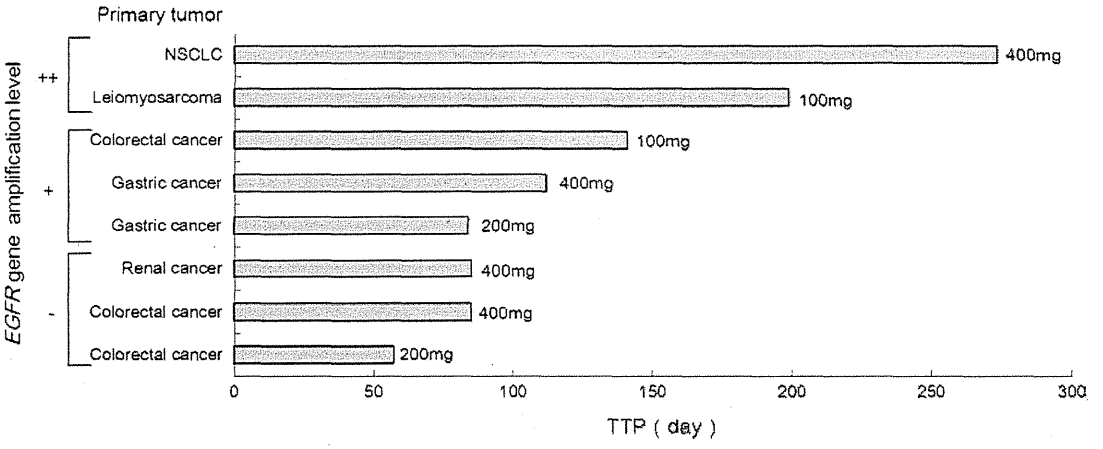


**Fig. 4** Time to progression by *EGFR* gene copy number level

bevacizumab or trastuzumab. The relatively short $t_{1/2}$ may suggest weekly dosing is necessary for nimotuzumab. If nimotuzumab is used in combination with other chemotherapy which has long $t_{1/2}$, the dosing schedule should be set with careful consideration.

PD analysis on EGFR and downstream signaling pathway components was conducted using skin tissue at pre- and on-treatment in order to investigate a biological effective dose. There was no correlation between the changes of molecules and nimotuzumab doses. These findings were similar to the previous phase I studies [10, 16]. Considering the thesis of biding property of nimotuzumab [14, 15], skin tissue may not be appropriate for PD analysis. It might be preferable to use tumor tissue for the future PD study.

The *EGFR* gene copy number status was measured by FISH method with 8 patient's tumor tissues. It was considered that TTP correlated with the FISH score positively. Consistent with our results, previous study has shown that an increased *EGFR* gene copy number detected by FISH was associated with better outcomes in non-small cell lung cancer patients receiving chemotherapy with cetuximab [25]. In addition, the recent clinical study of nimotuzumab with Japanese and Korean gastric cancer patients reported the positive correlation between efficacy, and both EGFR protein expression level and gene copy number status [20]. Based on the theory that bivalent binding is required to establish stable attachment of nimotuzumab to the cellar surface, high EGFR surface density may be desirable for

pharmacological action of nimotuzumab. However, no correlation between efficacy and EGFR expression level was found in this study. *EGFR* gene copy number is reported to correlate with EGFR protein expression on the cell surface [27]; however, our study exhibited that the FISH score was not correlated with EGFR expression level determined by IHC as shown in Online Resource 3. The possible reasons for the discrepancy of results between FISH and IHC seem to be the variety of the tumor types, fixation method, and condition of tumor samples. Further investigation into the predictive biomarker of nimotuzumab is warranted in the future study.

In conclusion, nimotuzumab administered weekly is well tolerated up to 400 mg in Japanese patients. These results support that 400 mg weekly administration might be recommended for further clinical studies, especially for nimotuzumab monotherapy. The property of low dermatological toxicity could be a preferable profile as an anti-EGFR mAbs. Our results support the further evaluation of nimotuzumab including biomarker exploration in the following phase II studies.

**Acknowledgments** The authors would like to thank all the patients who participated in this study as well as Hiroshi Terakawa, Kenji Hirotani, Yuko Aramaki, Kiyo Nishimoto, Taiga Takagi and Koji Ishizuka in DAIICHI SANKYO CO., LTD. (Tokyo, Japan) for the assistance. This study was supported by DAIICHI SANKYO CO., LTD. which provided study medication and assistance with data collection.

**Conflict of interest** Wataru Okamoto, Takayuki Yoshino, Toshiaki Takahashi, Isamu Okamoto, Shinya Ueda, Asuka Tsuya, Narikazu Boku, Kazuto Nishio, Masahiro Fukuoka, Nobuyuki Yamamoto, and Kazuhiko Nakagawa received a research funding for conducting this study from DAIICHI SANKYO CO., LTD. Masahiro Fukuoka and Narikazu Boku received lecture fees from DAIICHI SANKYO CO., LTD.

## References

1. Pal SK, Pegram M (2005) Epidermal growth factor receptor and signal transduction: potential targets for anti-cancer therapy. Anticancer Drugs 16:483–494
2. Rivera F, Vega-Villegas ME, Lopez-Brea MF, Marquez R (2008) Current situation of panitumumab, matuzumab, nimotuzumab and zalutumumab. Acta Oncol 47:9–19
3. Shawnta C, Aminah J (2010) STEPP for the EGFR inhibitor–induced rash—definitely a step in the right direction. Curr Oncol Rep 12:223–225
4. Racca P, Fanchini L, Caliendo V, Ritorto G, Evangelista W, Volpatto R, Milanesi E, Ciorba A, Paris M, Facilissimo I, Macripò G, Clerico M, Ciuffreda L (2008) Efficacy and skin toxicity management with cetuximab in metastatic colorectal cancer: outcomes from an oncologic/dermatologic cooperation. Clin Colorectal Cancer 7(1):48–54
5. Pinto C, Barone CA, Girolomoni G, Russi EG, Merlano MC, Ferrari D, Maiello E (2011) Management of skin toxicity associated with cetuximab treatment in combination with chemotherapy or radiotherapy. Oncologist 16:228–238
6. Crombet T, Rak J, Pérez R, Viloria-Petit A (2002) Antiproliferative, antiangiogenic, and proapoptotic activity of H-R3: a humanized anti-EGFR antibody. Int J Cancer 101:567–575
7. Maceira M, Rengifo E, Cedeño M, Merino N, Parada AC (2004) Immunohistochemical recognition of the epidermal growth factor receptor by the h-R3 antibody in the skin of experimental animals. Appl Immunohistochem Mol Morphol 12(4):360–363
8. Akashi Y, Okamoto I, Iwasa T, Yoshida T, Suzuki M, Hatashita E, Yamada Y, Satoh T, Fukuoka M, Ono K, Nakagawa K (2008) Enhancement of the antitumor activity of ionising radiation by nimotuzumab, a humanised monoclonal antibody to the epidermal growth factor receptor, in non-small cell lung cancer cell lines of differing epidermal growth factor receptor status. Br J Cancer 98:749–755
9. Basavaraj C, Sierra P, Shivu J, Melarkode R, Montero E, Nair P (2010) Nimotuzumab with chemoradiation confers survival advantage in treatment naïve head and neck tumors overexpressing EGFR. Cancer Biol Ther 10(7):673–681
10. Rojo F, Gracias E, Villena N, Cruz T, Corominas JM, Corradino I, Cedeño M, Campas C, Osorio M, Iznaga N, Bellosillo B, Rovira A, Marsoni S, Gascon P, Serrano S, Sessa C, Crombet T, Albanell J (2010) Pharmacodynamic trial of nimotuzumab in unresectable squamous cell carcinoma of the head and neck: a SENDO foundation study. Clin Cancer Res 16(8):2474–2482
11. Crombet T, Osorio M, Cruz T, Roca C, Castillo R, Mon R, Iznaga-Escobar N, Figueredo R, Koropatnick J, Renginfo E, Ferna'ndez E, Alva'rez D, Torres O, Ramos M, Leonard I, Pérez R, Lage A (2004) Use of the humanized anti-epidermal growth factor receptor monoclonal antibody h-R3 in combination with radiotherapy in the treatment of locally advanced head and neck cancer patients. J Clin Oncol 22(9):1646–1654
12. Rodríguez MO, Rivero TC, Bahi RC, Muchuli CR, Bilbao MA, Vinageras EN, Alert J, Galainena JJ, Rodríguez E, Gracias E, Mulén B, Wilkinson B, Armas EL, Pérez K, Pineda I, Frómeta M, Leonard I, Mullens V, Viada C, Luaces P, Torres O, Iznaga N, Crombet T (2010) Nimotuzumab plus radiotherapy for unresectable squamous-cell carcinoma of the head and neck cancer. Biol Ther 9(5):343–349
13. Crombet T, Figueredo J, Catala M, González S, Selva JC, Cruz TM, Toledo C, Silva S, Pestano Y, Ramos M, Leonard I, Torres O, Marinello P, Pérez R, Lage A (2006) Treatment of high-grade glioma patients with the humanized anti-epidermal growth factor receptor (EGFR) antibody h-R3. Cancer Biol Ther 5(4):375–379
14. Talavera A, Friemann R, Gómez-Puerta S, Martinez-Fleites C, Garrido G, Rabasa A, López-Requena A, Pupo A, Johansen RF, Sa'nchez O, Krengel U, Morenoet E (2009) Nimotuzumab, an antitumor antibody that targets the epidermal growth factor receptor, blocks ligand binding while permitting the active receptor conformation. Cancer Res 69(14):5851–5859
15. Garrido G, Tikhomirov IA, Rabasa A, Yang E, Gracia E, Iznaga N, Fernández LE, Crombet T, Kerbel RS, Pérez R (2011) Bivalent binding by intermediate affinity of nimotuzumab: a contribution to explain antibody clinical profile. Cancer Biol Ther 11(4):373–382
16. You B, Brade A, Magalhaes JM, Siu LL, Oza A, Lovell S, Wang L, Hedley DW, Nicacio LV, Chen EX (2011) A dose-escalation phase I trial of nimotuzumab, an antibody against the epidermal growth factor receptor, in patients with advanced solid malignancies. Invest New Drugs 29(5):996–1003
17. Crombet T, Torres L, Neninger E, Catala' M, Solano ME, Perera A, Torres O, Iznaga N, Torres F, Pérez R, Lage A (2003) Pharmacological evaluation of humanized anti-epidermal growth factor receptor, monoclonal antibody h-R3, patients with advanced epithelial-derived cancer. J Immunother 26(2):139–148
18. Cappuzzo F, Hirsch FR, Rossi E, Bartolini S, Ceresoli GL, Bemis L, Haney J, Witta S, Danenberg K, Domenichini I, Ludovini V,

Magrini E, Gregorc V, Doglioni C, Sidoni A, Tonato M, Franklin WA, Crino L, Bunn PA Jr, Varella-Garcia M (2005) Epidermal growth factor receptor gene and protein and gefitinib sensitivity in non–small-cell lung cancer. Nat Cancer Inst 97(9):643–655

19. Tsao MS, Sakurada A, Cutz JC, Zhu CQ, Kamel-Reid S, Squire J, Lorimer I, Zhang T, Liu N, Daneshmand M, Marrano P, Santos GC, Lagarde A, Richardson F, Seymour L, Whitehead M, Ding K, Pater J, Shepherd FA (2005) Erlotinib in lung cancer—molecular and clinical predictors of outcome. N Engl J Med 353(2):133–144
20. Kim YH, Sasaki Y, Lee KH, Rha SY, Park S, Boku N, Komatsu Y, Kim T, Kim S, Sakata Y (2011) Randomized phase II study of nimotuzumab, an anti-EGFR antibody, plus irinotecan in patients with 5-fluorouracil-based regimen-refractory advanced or recurrent gastric cancer in Korea and Japan: preliminary results. ASCO GI poster session abstract 87
21. Knijn N, Tol J, Koopman M, Werter MJBP, Imholz ALT, Valster FAA, Mol L, Vincent AD, Teerenstra S, Punt CJA (2011) The effect of prophylactic calcium and magnesium infusions on the incidence of neurotoxicity and clinical outcome of oxaliplatin-based systemic treatment in advanced colorectal cancer patients. Eur J Cancer 47:369–374
22. Bodnar L, Wcislo G, Gasowska-Bodnar A, Synowiec A, Szarlej-Wcisło K, Szczylika C (2008) Renal protection with magnesium subcarbonate and magnesium sulphate in patients with epithelial ovarian cancer after cisplatin and paclitaxel chemotherapy: a randomised phase II study. Eur J Cancer 44:2608–2614
23. Cao Y, Liao C, Tan A, Liu L, Gao F (2010) Meta-analysis of incidence and risk of hypomagnesemia with cetuximab for advanced cancer. Chemotherapy 56:459–465
24. Fernandez A, Spitzer E, Perez R, Boehmer FD, Eckert K, Zschiesche W, Grosse R (1992) A new monoclonal antibody for detection of EGF-receptors in western blots and paraffin-embedded tissue sections. J Cel Biochem 49(2):157–165
25. Hirsch FR, Herbst RS, Olsen C, Chansky K, Crowley J, Kelly K, Franklin WA, Bunn PA Jr, Varella-Garcia M, Gandara DR (2008) Increased *EGFR* gene copy number detected by fluorescent in situ hybridization predicts outcome in non–small-cell lung cancer patients treated with cetuximab and chemotherapy. J Clin Oncol 26(20):3351–3357
26. Boland WK, Bebb G (2009) Nimotuzumab: a novel anti-EGFR monoclonal antibody that retains anti-EGFR activity while minimizing skin toxicity. Expert Opin Biol Ther 9(9):1–7
27. Kimura M, Tsuda H, Morita D, Ichikura T, Ogata S, Aida S, Yoshizumi Y, Maehara T, Mochizuki H, Matsubara O (2004) A proposal for diagnostically meaningful criteria to classify increased epidermal growth factor receptor and c-erbB-2 gene copy numbers in gastric carcinoma, based on correlation of fluorescence in situ hybridization and immunohistochemical measurements. Virchows Arch 445(3):255–262

VOLUME 31 · NUMBER 26 · SEPTEMBER 10 2013

JOURNAL OF CLINICAL ONCOLOGY

DIAGNOSIS IN ONCOLOGY

# Acute Lung Injury With Alveolar Hemorrhage As Adverse Drug Reaction Related to Crizotinib

## Introduction

Crizotinib (Xalkori; Pfizer, New York, NY), a small molecule tyrosine kinase inhibitor, was approved by the US Food and Drug Administration and the Japansese Ministry of Health, Labor, and Welfare for the treatment of patients with advanced non–small-cell lung cancer (NSCLC) harboring a rearrangement in the anaplastic lymphoma kinase (*ALK*) gene. Marked response to crizotinib was demonstrated in patients with ALK fusion–bearing lung cancer, and the most common adverse events associated with crizotinib treatment were nausea, diarrhea, and visual disturbances, most of which were mild.[1,2] In a phase II study, eight (< 1%) patients discontinued the treatment due to the development of pneumonitis.[3] Here we present, to our knowledge, the first case report of an acute life-threatening lung injury associated with crizotinib therapy.

## Case Report

A 63-year-old male former smoker had undergone a left lower lobectomy with systematic lymph node dissection for pulmonary adenocarcinoma (papillary adenocarcinoma, moderately differentiated with a micropapillary component, pT1aN2M0 stage IIIA) in October 2004. Four years later, tumor recurrence occurred in a subcarinal lymph node (#7). For two years, the lymph node grew gradually in size, and a new lesion was detected in the right lower lobe (S10). The histologic and molecular profiles of the resected tumor were reviewed and fluorescent in situ hybridization analysis demonstrated an echinoderm microtubule-associated protein-like 4 (EML 4) –ALK rearrangement. He was administered systemic chemotherapy as follows: four cycles of cisplatin and pemetrexed as first-line chemotherapy (between May 17 and August 12, 2010), and two cycles of docetaxel as second-line chemotherapy (between July 21 and August 10, 2011). Docetaxel treatment was discontinued due to hematologic toxicity. Thereafter, the disease progressed with the growth of #7 and S10 lesions. Crizotinib treatment (250 mg orally BID.) was initiated on December 13, 2011. Concomitant medications while on crizitinib were lansoprazole (15 mg, QD), warfarin potassium (1.5 mg, QD), thiamazole (5 mg, QD, alternate-day administration), and magnesium oxide (330 mg, TID). After 7 weeks of treatment, on January 31, 2012, the patient developed pyrexia (38°C), progressive dyspnea, and a cough with hemoptysis, and he was admitted to the emergency room. Examination of his vital signs revealed a temperature of 38.1°C, blood pressure of 115/55 mmHg, pulse of 86 beats/min, and respiratory rate of 24 breaths/min. Inspiratory crackles were audible in the right lung fields. With the patient breathing via a mask with oxygen supplementation at a flow rate of 10 l/min, arterial blood gas analysis revealed an arterial oxygen pressure of 50.5 torr, a carbon dioxide arterial pressure of 61.7 torr, and pH of 7.42. Chest x-ray revealed extensive bilateral diffuse pulmonary infiltration (Fig 1A). Chest computed tomography (CT) revealed bilateral, predominantly dependent and diffuse ground-grass attenuation (Fig 1B), reverse butterfly shadow (Fig 1C).

A CBC showed a WBC count of 10,590/$\mu$L (85% segmented neutrophils, 0.2% eosinophils, and 8% lymphocytes), serum hemoglobin of 13.1 g/dL, and an international normalized ratio of prothrombin time of 1.9, with no evidence of coagulation abnormalities. The serum level of C-reactive protein (15.2 mg/dL), creatinine (1.68 mg/dL), AST (70 IU/L), ALT (77 IU/L), lactate dehydrogenase (480 IU/L), creatine kinase (269 U/L), surfactant protein-D (179 ng/mL), and KL-6 (934 U/mL) were all elevated. Electrocardiography showed no abnormal findings and echocardiography revealed normal systolic function. Serologic data revealed no abnormal findings suggestive of collagen vascular diseases, sputum and blood cultures were negative. The patient was intubated and started on mechanical ventilatory support. Under the diagnosis of drug-induced acute lung injury (ALI)/acute respiratory distress syndrome (ARDS) and diffuse alveolar hemorrhage (DAH), we started the patient on treatment with high-dose intravenous methylprednisolone (1 g per day), broad-spectrum antibiotics, and sivelestat 0.20 mg/kg/hr. Fiberoptic bronchoscopy was performed, which revealed no evidence of *Pneumocystis carini* pneumonia, acid-fast bacilli, fungi or malignancy, and no abnormalities other than bronchial hemorrhage from right bronchus intermedius (*) in fiberoptic bronchoscopy (Fig 2).

By day 8 after admission, the respiratory status improved, with increase of the arterial oxygen pressure to 125 torr under a fraction of inspiratory oxygen 30%, and we decided to extubate the patient. However after day 8 (hospital day 11) of administration of prednisolone at 60 mg per day (intravenous), the respiratory status and radiographic findings began to worsen. The patient was reintubated and started again on mechanical ventilatory support. Despite the higher-dose prednisolone treatment for the ALI/ARDS, the patient's respiratory status and radiographic findings continued to worsen. Respiratory acidosis began to become more severe as a result of the high fraction of inspiratory oxygen. On hospital day 40, the patient died of multiple organ failure under a do-not-resuscitate order. An autopsy was performed with the consent of the next of kin.

*Autopsy results.* The right lung was increased in weight (925 g), while the left lung was atrophic with severe pleural adhesions. Histological examination of the lung tissue confirmed the presence of metastatic adenocarcinoma in the right hilar lymph nodes. High-sensitive immunohistochemical analysis revealed positive staining for ALK. No malignant cells were found in other organs, such as the liver or kidney. Diffuse fibroproliferative-phase alveolar damage (DAD), with organization in the alveolar spaces, and thickened alveolar septa with fibroblastic proliferation were observed in the areas corresponding to the bilateral, predominantly dependent and diffuse ground-grass attenuation on CT (Fig 3). No evidence of infection or of other specific etiologies was found.

## Discussion

Numerous cytotoxic chemotherapeutic agents have been reported to exert pulmonary toxicity.[4] The diagnosis of drug-associated interstitial lung disease (ILD) involves three elements: clinical suspicion,

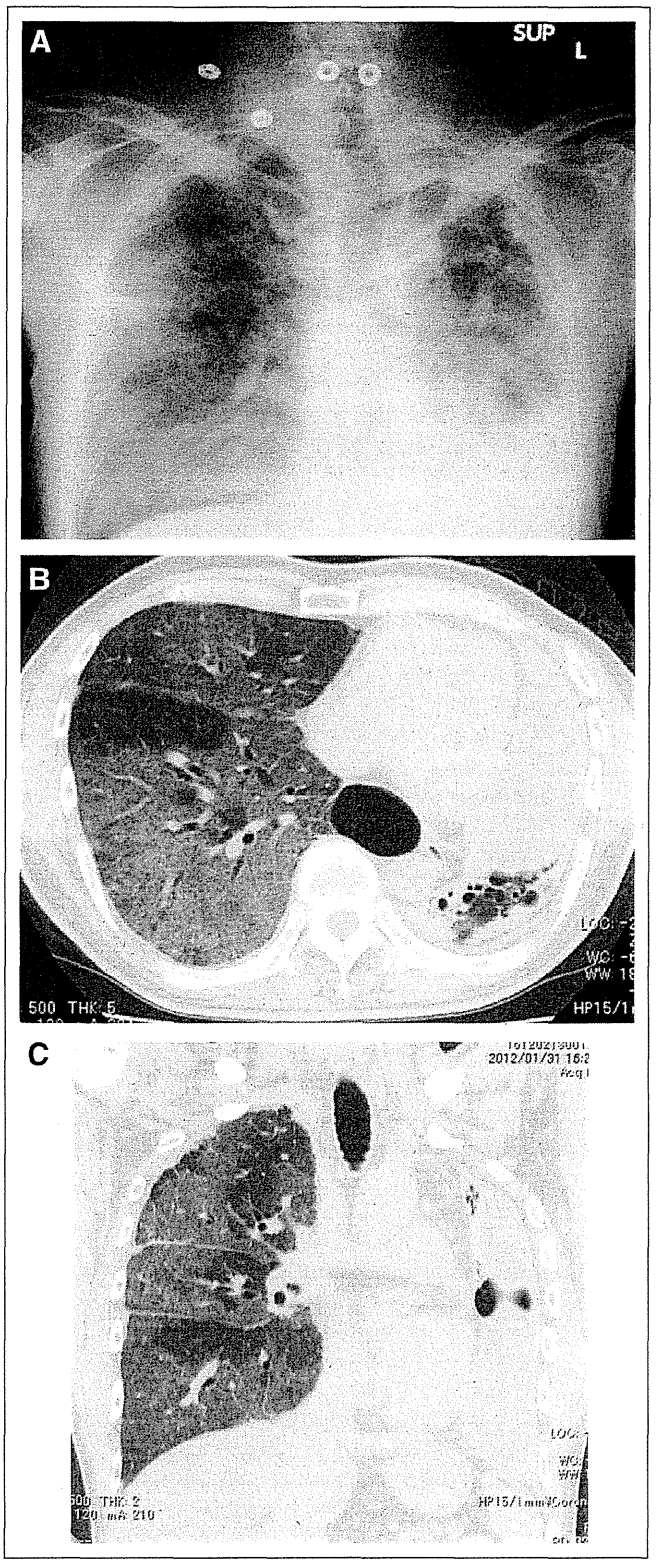


Fig 1.

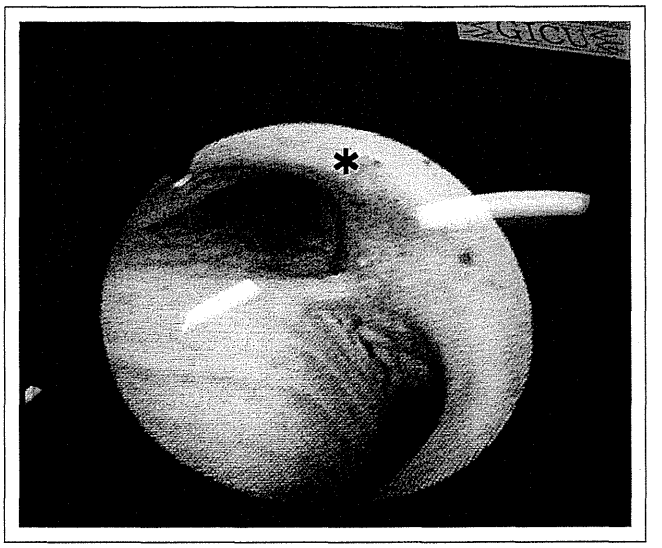

Fig 2.

combined with methodical exclusion of other potential etiologies, differentiation from other parenchymal lung diseases on CT, and a compatible histological pattern. There are no specific radiological patterns of parenchymal changes associated with drug-induced ILD. The lung reactions can be divided into five main types: DAD, hypersensitivity reaction, nonspecific interstitial pneumonia, organizing pneumonia, and eosinophilic pneumonia.[5] Diffuse forms of drug-induced ILD include processes that mimic ARDS and DAH. These patterns of drug-induced ILD are especially common in patients receiving cytotoxic chemotherapeutic agents.[6] Among the biologics, gefitinib has been reported to cause severe drug-induced ILD.[7,8,9] The prevalence of gefitinib-induced ILD has been reported as 3.5%, with mortality of 1.6%.[10] DAD usually develops a few weeks or months after the initiation of therapy. It can progress to a fibroproliferative phase over a relatively short period of time.[6] The mechanisms of damage include direct pulmonary toxicity and indirect effects via stimulation of inflammatory reactions.[11] The mechanism underlying the induction of alveolar damage by crizotinib remains unclear.

DAH is mainly caused by damage of the alveolar microcirculation. In most cases, DAH is associated with pulmonary capillaritis.[12] DAH without capillaritis can be caused by various disorders[13], and the majority of patients with DAH presenting with the features of ALI/ARDS have no underlying connective tissue diseases.[14] Some drugs may cause DAD manifesting features of ARDS, and of DAH in severe cases.[15] In this case, there were no evidence for pulmonary capillaritis, or connective tissue disease.

Starting with pyrexia, he developed rapidly progressive dyspnea with severe hypoxia and diffuse interstitial infiltrates on radiographic studies 49 days after beginning treatment with crizotinib. The course of clinical and radiographical finding consisted with autopsy finding in fibroproliferative-phase DAD. There were no infectious and lymphangitic spread findings. His history of clinical examination did not provide any evidence of toxic origin, prior radiotherapy, or collagen vascular disease. He has no pre-existing liver dysfunction. The clinical course, pathological findings, and exclusion of these other causes indicated that the ALI with DAD was probably attributable to crizotinib.

Crizotinib is an oral, potent, and selective small-molecule competitive inhibitor of ALK, with additional anti-MET[16] and ROS[17] activity. On the basis of its demonstrated efficacy and safety in phase I and phase II studies, crizotinib was granted accelerated approval by the US Food and Drug Administration for use in the treatment of

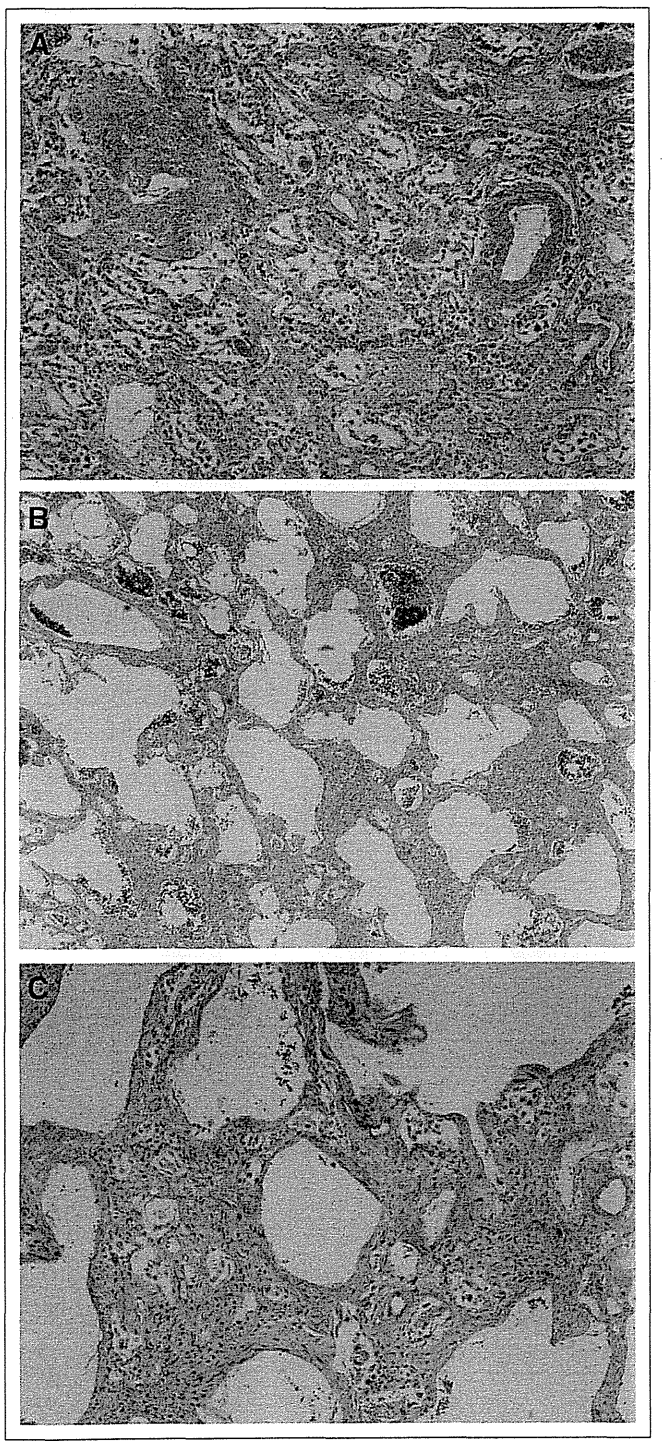


Fig 3.

advanced, ALK-positive NSCLC. Common adverse events of crizotinib include mild transient visual disorders, mild GI toxicities, fatigue, with elevation of the serum ALT levels occurring rarely, and pneumonitis occurring even more rarely (1.6%).[18]

It will be important to determine if there might be any risk factors for the induction of pneumonitis by crizotinib, such as gender, ethnicity, comorbidities, smoking history, prior radiation, or other factors. The clinical history, histological evidence of lung injury, and exclusion of other potential factors suggested that the lung injury was caused by crizotinib.

This is the first case of pathologically proven lung injury caused by crizotinib. Thus, the potential of crizotinib to cause life-threatening pulmonary toxicity must be recognized, and careful monitoring of the patients' clinical course for any relevant symptoms is important during treatment with crizotinib.

*Akira Ono, Toshiaki Takahashi, Takuma Oishi, Takashi Sugino, Hiroaki Akamatsu, Takehito Shukuya, Tetsuhiko Taira, Hirotsugu Kenmotsu, Tateaki Naito, Haruyasu Murakami, Takashi Nakajima, Masahiro Endo, and Nobuyuki Yamamoto*

Shizuoka Cancer Center, Shizuoka, Japan

## AUTHORS' DISCLOSURES OF POTENTIAL CONFLICTS OF INTEREST

The author(s) indicated no potential conflicts of interest.

## REFERENCES

1. Kwak EL, Bang YJ, Camidge DR, et al: Anaplastic lymphoma kinase inhibition in non-small-cell lung cancer. N Engl J Med 363:1693-1703, 2010
2. Camidge DR, Bang YJ, Kwak EL, et al: Activity and safety of crizotinib in patients with ALK-positive non-small-cell lung cancer: Updated results from a phase 1 study. Lancet Oncol 13:1011-1019, 2012
3. Kim D-W, Ahn M-J, Shi Y, et al: Results of a global phase II study with crizotinib in advanced ALK-positive non–small-cell lung cancer (NSCLC). J Clin Oncol 30:15, 2012 (suppl; abstr 7533)
4. Rosenow EC 3rd, Limper AH: Drug-induced pulmonary disease. Semin Respir Infect 10:86-95, 1995
5. Müller NL, White DA, Jiang H, et al: Diagnosis and management of drug-associated interstitial lung disease. Br J Cancer 91:S24-S30, 2004
6. Myers JL, Limper AH, Swensen SJ: Drug-induced lung disease: A pragmatic classification incorporating HRCT appearances. Semin Respir Crit Care Med 24:445-454, 2003
7. Inoue A, Saijo Y, Maemondo M, et al: Severe acute interstitial pneumonia and gefitinib. Lancet 361:137-139, 2003
8. Okamoto I, Fujii K, Matsumoto M, et al: Diffuse alveolar damage after ZD1839 therapy in a patient with non-small cell lung cancer. Lung Cancer 40:339-342, 2003
9. Ieki R, Saitoh E, Shibuya M: Acute lung injury as a possible adverse drug reaction related to gefitinib. Eur Respir J 22:179-181, 2003
10. Ando M, Okamoto I, Yamamoto N, et al: Predictive factors for interstitial lung disease, antitumor response, and survival in non–small-cell lung cancer patients treated with gefitinib. J Clin Oncol 24:2549-2556, 2006
11. Higenbottam T, Kuwano K, Nemery B, et al: Understanding the mechanisms of drug-associated interstitial lung disease. Br J Cancer 91:S31-S37, 2004
12. Travis WD, Colby TV, Lombard C, et al: A clinicopathologic study of 34 cases of diffuse pulmonary hemorrhage with lung biopsy confirmation. Am J Surg Pathol 14:1112-1125, 1990
13. Collard HR, Schwarz MI: Diffuse alveolar hemorrhage. Clin Chest Med 25:583-592, 2004
14. Jin SM, Yim JJ, Yoo CG, et al: Aetiologies and outcomes of diffuse alveolar haemorrhage presenting as acute respiratory failure of uncertain cause. Respirology 14:290-294, 2009
15. Green RJ, Ruoss SJ, Kraft SA, et al: Pulmonary capillaritis and alveolar hemorrhage: Update on diagnosis and management. Chest 110:1305-1316, 1996
16. Christensen JG, Zou HY, Arango ME, et al: Cytoreductive antitumor activity of PF-2341066, a novel inhibitor of anaplastic lymphoma kinase and c-Met, in experimental models of anaplastic large-cell lymphoma. Mol Cancer Ther 6:3314-3322, 2007
17. Bergethon K, Shaw AT, Ou SH, et al: ROS1 rearrangements define a unique molecular class of lung cancers. J Clin Oncol 30:863-870, 2012
18. Xalkori (crizotinib, package insert). New York, NY, Pfizer, 2011

DOI: 10.1200/JCO.2012.47.1110; published online ahead of print at www.jco.org on July 15, 2013



 

OPEN ACCESS Freely available online

PLOS | ONE

# Size-Based Isolation of Circulating Tumor Cells in Lung Cancer Patients Using a Microcavity Array System

**Masahito Hosokawa[1,2], Hirotsugu Kenmotsu[3], Yasuhiro Koh[2], Tomoko Yoshino[1], Takayuki Yoshikawa[1], Tateaki Naito[3], Toshiaki Takahashi[3], Haruyasu Murakami[3], Yukiko Nakamura[3], Asuka Tsuya[3], Takehito Shukuya[3], Akira Ono[3], Hiroaki Akamatsu[3], Reiko Watanabe[4], Sachiyo Ono[4], Keita Mori[5], Hisashige Kanbara[6], Ken Yamaguchi[2], Tsuyoshi Tanaka[1], Tadashi Matsunaga[1], Nobuyuki Yamamoto[3]***

**1** Division of Biotechnology and Life Science, Institute of Engineering, Tokyo University of Agriculture and Technology, Tokyo, Japan, **2** Drug Discovery and Development Division, Shizuoka Cancer Center Research Institute, Shizuoka, Japan, **3** Division of Thoracic Oncology, Shizuoka Cancer Center, Shizuoka, Japan, **4** Division of Diagnostic Pathology, Shizuoka Cancer Center, Shizuoka, Japan, **5** Clinical Trial Coordination Office, Shizuoka Cancer Center, Shizuoka, Japan, **6** Hitachi Chemical Co., Ltd., Tokyo, Japan

## Abstract

***Background:*** Epithelial cell adhesion molecule (EpCAM)-based enumeration of circulating tumor cells (CTC) has prognostic value in patients with solid tumors, such as advanced breast, colon, and prostate cancer. However, poor sensitivity has been reported for non-small cell lung cancer (NSCLC). To address this problem, we developed a microcavity array (MCA) system integrated with a miniaturized device for CTC isolation without relying on EpCAM expression. Here, we report the results of a clinical study on CTCs of advanced lung cancer patients in which we compared the MCA system with the CellSearch system, which employs the conventional EpCAM-based method.

***Methods:*** Paired peripheral blood samples were collected from 43 metastatic lung cancer patients to enumerate CTCs using the CellSearch system according to the manufacturer's protocol and the MCA system by immunolabeling and cytomorphological analysis. The presence of CTCs was assessed blindly and independently by both systems.

***Results:*** CTCs were detected in 17 of 22 NSCLC patients using the MCA system versus 7 of 22 patients using the CellSearch system. On the other hand, CTCs were detected in 20 of 21 small cell lung cancer (SCLC) patients using the MCA system versus 12 of 21 patients using the CellSearch system. Significantly more CTCs in NSCLC patients were detected by the MCA system (median 13, range 0–291 cells/7.5 mL) than by the CellSearch system (median 0, range 0–37 cells/7.5 ml) demonstrating statistical superiority ($p = 0.0015$). Statistical significance was not reached in SCLC though the trend favoring the MCA system over the CellSearch system was observed ($p = 0.2888$). The MCA system also isolated CTC clusters from patients who had been identified as CTC negative using the CellSearch system.

***Conclusions:*** The MCA system has a potential to isolate significantly more CTCs and CTC clusters in advanced lung cancer patients compared to the CellSearch system.

**Citation:** Hosokawa M, Kenmotsu H, Koh Y, Yoshino T, Yoshikawa T, et al. (2013) Size-Based Isolation of Circulating Tumor Cells in Lung Cancer Patients Using a Microcavity Array System. PLoS ONE 8(6): e67466. doi:10.1371/journal.pone.0067466

**Editor:** William C S Cho, Queen Elizabeth Hospital, Hong Kong

**Received** January 18, 2013; **Accepted** May 17, 2013; **Published** June 28, 2013



**Funding:** This work was partly supported by the Regional Innovation Cluster Program and a Grant-in-Aid for Research Fellowship for Young Scientists (11J11150) from the Ministry of Education, Culture, Sports, Science and Technology of Japan. The funders had no role in study design, data collection and analysis, decision to publish, or preparation of the manuscript.

**Competing Interests:** MH, TYoshino, HKanbara, and TM have applied for patents related to the MCA system. HKanbara is employed by Hitachi Chemical Co., Ltd. This does not alter the authors' adherence to all the PLOS ONE policies on sharing data and materials.

* E-mail: n.yamamoto@scchr.jp

## Introduction

Lung cancer is the leading cause of cancer-related death in most industrialized countries. Small cell lung cancer (SCLC) accounts for approximately 15% of lung cancer cases, and non-small cell lung cancer (NSCLC), which includes adenocarcinoma (ADC) and squamous cell carcinoma (SCC), accounts for 85% of lung cancer cases. It has recently been shown that identification of NSCLC patients by detection of genetic aberrations, specifically *EGFR*-activating mutations and the *EML4-ALK* fusion gene, allows for better prediction of response to EGFR tyrosine kinase inhibitors and ALK inhibitors, respectively [1,2]. Despite advances in prevention and treatment, NSCLC patients are often diagnosed at an advanced stage and have a poor prognosis due to the disease's tendency toward distant metastasis, the primary cause of mortality among NSCLC patients. Characterized by aggressive tumor growth and often presenting with metastases in the regional nodes and distant organs, SCLC is initially highly sensitive to chemotherapy but tends to acquire chemoresistance, leading to inevitable relapse.

Circulating tumor cells (CTCs) are defined as tumor cells circulating in the peripheral blood of patients with metastatic cancer. When measured using the US Food and Drug Adminis-

tration (FDA)-approved CellSearch system (Veridex, Raritan, NJ, USA), the number of CTCs in peripheral blood can be used to predict the prognosis of patients with metastatic breast cancer [3], colorectal cancer [4], prostate cancer [5], NSCLC [6], and SCLC [7]. The CellSearch system enriches CTCs using magnetic beads coated with a monoclonal antibody-targeting epithelial cell marker, such as the epithelial cell-adhesion molecule (EpCAM) [8,9]. However, several studies have shown that the presence of EpCAM on tumor cells varies with tumor type [10,11]. The expression of epithelial cell markers, including EpCAM, is downregulated to increase invasiveness and metastatic potential by epithelial-to-mesenchymal transition (EMT) [12–16]. It has been suggested that the low prevalence of CTCs detected in patients with advanced NSCLC using the CellSearch system may be due to the loss of EpCAM expression [17], indicating that EpCAM-based CTC isolation methods cannot achieve stable and reproducible CTC recovery from all tumor types.

Other CTC isolation methods are mainly based on differences in the size and deformability between CTCs and hematologic cells. As tumor cells (>8 μm) are larger than leukocytes [18–21], isolation by size of epithelial tumor cells (ISET) can be achieved using filtration to separate individual cells. ISET using a polycarbonate filter, an inexpensive, user-friendly method of enriching CTCs, enables the recovery and detection of epithelial-marker-negative CTCs on the basis of size-dependent CTC isolation. In clinical tests, use of an ISET-based system has been found to achieve higher CTC detection sensitivity in patients with metastatic lung cancer compared to use of the CellSearch system [22–24].

Recently, microfabricated devices for size-based separation of tumor cells have been widely developed to enable precise and efficient enrichment of CTCs from whole blood [25–28]. These devices include a miniaturized microcavity array (MCA) system that we developed for the highly efficient entrapment of single cells by filtration based on differences in the sizes of cells [29,30]. In a previous study, we examined the application of our MCA system to the detection of spiked tumor cells from unprocessed human whole blood based on differences in the size and deformability between tumor cells and other blood cells [31]. Using our device, we were able to entrap tumor cells onto size- and geometry-controlled microcavity arrays composed of 10,000 apertures by applying negative pressure, allowing the entrapped cells to be easily enumerated and analyzed by microscopic imaging of specified areas. Furthermore, we found that use of the miniaturized device allowed for introduction of a series of reagents for detection of tumor cells through the microfluidic structure. Our results indicate that our system is a simple yet precise system for the detection of tumor cells within whole blood. To confirm and build on our previous findings, we compared the capacity and efficiency of our novel MCA system and the current gold standard CellSearch system in performing CTC detection and enumeration in whole blood samples drawn from a cohort of NSCLC and SCLC patients.

## Materials and Methods

### Study Design and Ethics Statement

This prospective study was conducted to evaluate CTC enumeration using the CellSearch system and the MCA system in patients with metastatic lung cancer in a blinded experiment (UMIN clinical trial registry, number UMIN000005189). The presence of CTCs was assessed individually according to their criteria before knowing any results from each other. The study inclusion criteria were diagnosis of pathologically proven lung cancer with radiologically evident metastatic lesions, i.e., histologically or cytologically confirmed metastatic NSCLC or SCLC, and enrollment at the Shizuoka Cancer Center. The institutional review boards of the Shizuoka Cancer Center approved the study protocol, and all patients provided written informed consent. From each of the 43 patients who were enrolled, among whom 22 had been diagnosed with NSCLC and 21 with SCLC, 10–15 mL of blood was collected in EDTA tubes for CTC enumeration by the MCA system in our laboratory (Shizuoka Cancer Center, Shizuoka, Japan) and 20 mL was collected in CellSave collection tubes for CTC enumeration by the CellSearch system in the laboratory of SRL Inc. (Tokyo, Japan).

### Cell Culture and Labeling

HCC827, NCI-H358, NCI-H441, DMS79, NCI-H69, and NCI-H82 cell lines were purchased from the American Type Culture Collection without further testing or authentication. A549 (Riken Bioresource Center, Tsukuba, Japan) and PC-14 [32] were kindly provided by Dr. Fumiaki Koizumi (National Cancer Center, Tokyo, Japan). The A549, HCC827, NCI-H358, NCI-H441, PC-14, DMS79, NCI-H69, and NCI-H82 NSCLC and SCLC cell lines were cultured in RPMI 1640 medium containing 2 mM of L-glutamine (Sigma-Aldrich, Irvine, UK), 10% (v/v) fetal bovine serum (FBS; Invitrogen Corp., Carlsbad, CA, USA), and 1% (v/v) penicillin/streptomycin (Invitrogen Corp.) for 3–4 days at 37°C with 5% $CO_2$ supplementation. Immediately prior to each experiment, cells grown to confluence were trypsinized and resuspended in phosphate-buffered saline (PBS). As a measurement of tumor cell size, cell size distribution was determined using the CASY® Cell Counter+Analyzer System Model TTC (Schärfe System GmbH, Reutlingen, Germany). To evaluate device performance, the tumor cell lines were labeled with CellTracker Red CMTPX (Molecular Probes, Eugene, OR, USA), with labeling achieved by incubating the cells with a tracking dye (5 μM) for 30 min. After the cells had been pelleted by centrifugation (200 g for 5 min), the supernatant was decanted. The cells were then washed twice with PBS to remove any excess dye before being resuspended in PBS containing 2 mM EDTA and 0.5% bovine serum albumin (BSA).

### Fabrication of the MCA System

The MCA system was fabricated in the same manner as previously reported [29,31]. For CTC enumeration with fluorescence microscope observation, an MCA that had been manufactured by electroforming of nickel was used. For CTC morphological analysis by Giemsa staining, a transparent MCA that had been manufactured by laser irradiation of poly(ethylene terephthalate) (PET) was used. Each of the 10,000 cavities arranged in each 100×100 array was fabricated to have a diameter of 8–9 μm at the top surface and to be 60 μm distant from the adjacent microcavity. Poly(dimethylsiloxane) (PDMS) structures were fabricated and then integrated with the MCA such that the upper substrate consisted of a microchamber, a sample inlet, and an outlet, while the lower substrate beneath the MCA contained a vacuum line to produce negative pressure, enabling cell entrapment. The CTC isolation device was constructed by assembling the MCA, while the upper and lower PDMS layers were constructed using spacer tapes (Figure 1a). The sample inlet was connected to a reservoir, while the vacuum microchannel was connected to a peristaltic pump.

### CTC Enumeration using the MCA System

Human blood samples were collected in a collection tube with EDTA to prevent coagulation and used within 2 h. The average

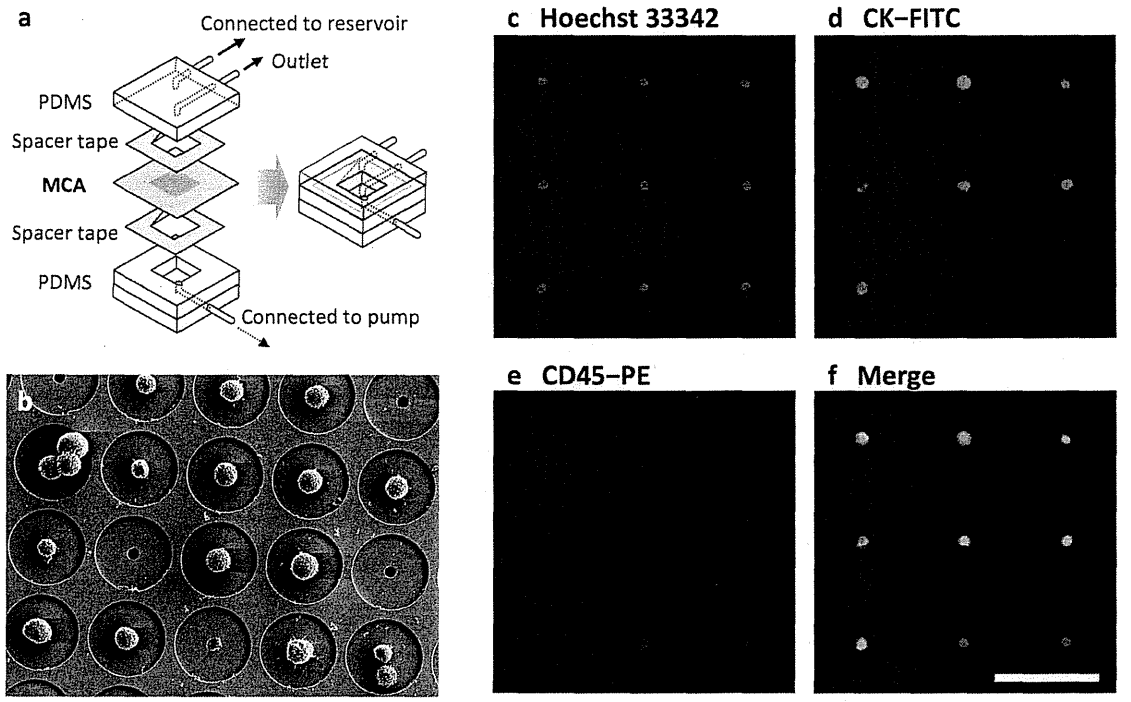


**Figure 1. MCA system for size-based isolation of CTCs.** (a) Schematic diagram of the structure of the MCA system. (b) Scanning electron microscope image of a cultured tumor cell line trapped on the MCA system. (c–f) Cells isolated from SCLC patient blood stained with Hoechst 33342 (c) and fluorescent-labeled antibodies that target cytokeratin (d) and CD45 (e). Merging of the images (f) allowed for identification of CTCs and hematologic cells. Scale bar = 60 μm.
doi:10.1371/journal.pone.0067466.g001

volume of blood analyzed was 4.0 mL per sample (range, 3.0–7.5 mL). All CTC enumeration using the MCA system was performed without knowledge of patient clinical status in the laboratory of the Shizuoka Cancer Center Research Institute. After introduction of blood samples into the reservoir, negative pressure was applied to a cell suspension using a peristaltic pump connected to a vacuum line, allowing the sample to be passed through the microcavities at a flow rate of 200 μL/min. To remove any blood cells remaining on the array, PBS containing 2 mM EDTA and 0.5% BSA (1 mL) was introduced into the reservoir and passed through the microcavities at a flow rate of 200 μL/min for 5 min.

To stain the CTCs with anti-pancytokeratin antibody, trapped cells were fixed by flowing 400 μL of 1% paraformaldehyde (PFA) in PBS through the MCA at a flow rate of 20 μL/min for 20 min. After washing with 100 μL of PBS, the cells were treated with 300 μL of 0.2% Triton X-100 in PBS at a flow rate of 20 μL/min for 15 min. After permeabilization, cells were treated with 3% BSA in PBS at a flow rate of 20 μL/min for 30 min. To identify CTCs and leukocytes, 600 μL of cell-staining solution containing 1 μg/mL of Hoechst 33342 (Molecular Probes); a cocktail of anti-pancytokeratin antibodies (Alexa488-AE1/AE3 (1:100 dilution; eBioscience, San Diego, CA, USA) and FITC-CK3-6H5 (1:60 dilution; Miltenyi Biotec, Auburn, California CA USA); and PE-labeled anti-CD45 antibody (1:120 dilution; BD Biosciences, San Jose, CA, USA) was flowed through the microcavities at a flow rate of 20 μL/min for 30 min. Finally, the array was washed with 400 μL of PBS containing 2 mM of EDTA and 0.5% BSA to remove any excess dye. After recovery of tumor cells, an image of the entire cell array area was obtained using a fluorescence microscope (BX61; Olympus Corporation, Tokyo, Japan) integrated with a 10× objective lens and a computer-operated motorized stage; WU, NIBA, and WIG filter sets; a cooled digital camera (DP-70; Olympus Corporation); and Lumina Vision acquisition software (Mitani Corporation, Tokyo, Japan).

In clinical trials, an entire image of the cell array area had been obtained using a fluorescence microscope (Axio Imager Z1; Carl Zeiss, Oberkochen, Germany) integrated with a 10× or 20× objective lens and a computer-operated motorized stage; WU, FITC, and Texas Red filter sets; a digital camera (AxioCam HRc; Carl Zeiss); and AxioVision acquisition software (Carl Zeiss). Subsequently, image analysis had been performed and objects that satisfied predetermined criteria had been counted. Fluorescent intensities and morphometric characteristics, such as cell size, shape, and nuclear size, were considered when performing CTC identification and non-tumor cell exclusion, with cells characterized by a round to oval morphology and a visible nucleus (i.e., as Hoechst-33342 positive) that were positive for cytokeratin and negative for CD45 identified as CTCs. Isolated CTCs on the transparent MCA were also stained using a May-Grünwald–Giemsa (MGG) staining method consisting of fixation with 4% PFA, undiluted May-Grünwald stain for 2 min, May-Grünwald stain diluted 50% in PBS for 1 min, and Giemsa stain for 18 min, followed by rinsing with PBS for 1 min.

## CTC Enumeration using the CellSearch System

Whole blood samples were maintained at room temperature, mailed overnight to the laboratory of SRL Inc., and processed within 96 h of collection. All CTC evaluations were performed without knowledge of patient clinical status in the laboratory and

the results were reported quantitatively as the number of CTCs/7.5 mL of blood. CTCs were defined as EpCAM-isolated intact cells showing positive staining for cytokeratin and negative staining for CD45. In accordance with previous evaluations of the CellSearch system [8], a patient was considered CTC positive if ≥2 CTCs/7.5 mL of blood were detected in the patient's sample.

## Results

### CTC Isolation and Image Analysis using the MCA System

Isolation and staining of the tumor cells from whole blood was completed within 120–180 min, and image scanning of the MCA was performed at 3 fluorescence wavelengths using a 10× or 20× objective lens and a motorized stage. Figure 1b–f shows the scanning electroscope microscopy (SEM) and fluorescence images of the stained cells that were recovered on the MCA. As can be observed, solitary cells and cell clusters were individually trapped and retained on the microcavities that could be easily enumerated. Recovered cells that had a round to oval morphology and a visible nucleus (i.e., were Hoechst 33342 positive) and were positive for pancytokeratin and negative for CD45 were identified as tumor cells, while CD45-positive cells were identified as contaminating normal hematologic cells. The images reveal the existence of a distinct immunophenotype of epithelial cell marker-positive tumor cells. Although a number of leukocytes were retained on the array, tumor-cell enumeration was relatively facile because individual cells had been trapped on the precisely aligned microcavities.

### Sensitivity of the MCA System in CTC Detection of Lung Cancer Cell Lines

In our previous study, varying numbers of cells of the lung cancer cell line NCI-H358 were spiked into blood, and tumor cell isolation was evaluated using our MCA system [31]. The calculated detection efficiency was constant and over 90% when 10–100 tumor cells were present per milliliter of blood. In this study, in order to evaluate the recovery efficiency of various lung cancer cell lines using the MCA system, 100 cells of each of 8 lung cancer cell lines (A549, HCC-827, NCI-H358, NCI-H441, PC-14, DMS-72, NCI-H69, and NCI-H82) were spiked into healthy donor blood samples and then processed by MCA assay. Table 1 shows the average recovery efficiency and typical diameter of the cell lines. As can be observed, a high recovery rate was obtained, regardless of tumor type, ranging from 68% to 100% in the cell line spike-in experiments. Most of the recovered cells were viable and able to proliferate even after undergoing the isolation process, suggesting the potential for further biological and molecular analysis of CTCs.

Next, in order to evaluate the specificity and sensitivity of CTCs detection, the sensitivity tests were performed on artificial samples prepared by adding 1 and 3 cultured NCI-H358 cells to healthy donor blood samples, as previously reported by Vona et al. [20]. One and 3 cultured NCI-H358 cells were spiked into separate 7.5 mL aliquots of blood. These 7.5 mL blood samples were processed with the MCA system in 3 independent tests (Table S1). The results demonstrated a sensitivity threshold for MCA system close to 1 tumor cell per 7.5 mL of blood. In addition, CTCs were not detectable from 6 healthy donor bloods using the MCA system (Figure 2). Therefore, a patient was considered CTC positive if ≥1 CTCs per 7.5 mL of blood was detected by the MCA system.

In addition, the tumor cell recovery efficiency of the MCA system was compared with that of ISET system (Figure S1). In this comparison, 100 cells of NSCLC cell line NCI-H358 was spiked into healthy donor blood samples and then processed by the MCA system and a track-etched polycarbonate 8-μm pore membrane (Nucleopore; Whatman Ltd., Kent, UK). The results revealed the recovery rate using the MCA system (100% ±5%) to be significantly higher than that using the ISET system (91% ±2%) ($p<0.05$, t-test), indicating that use of the MCA system enables CTC isolation with an efficiency equivalent to or greater than that of the ISET system.

**Table 1.** CTC recovery efficiency and average cell diameter.

| Cell line | Origin | Average cell diameter (μm) | Recovery efficiency (%) |
|---|---|---|---|
| A549 | NSCLC | 17.3 | 98±3 |
| HCC827 | NSCLC | 19.6 | 99±6 |
| NCI-H358 | NSCLC | 18.1 | 100±6 |
| NCI-H441 | NSCLC | 20.6 | 98±8 |
| PC-14 | NSCLC | 19.5 | 97±2 |
| DMS79 | SCLC | 14.1 | 76±1 |
| NCI-H69 | SCLC | 12.5 | 68±2 |
| NCI-H82 | SCLC | 13.5 | 80±4 |

Cells were spiked into 1 mL of normal blood and recovered using the MCA system.
doi:10.1371/journal.pone.0067466.t001

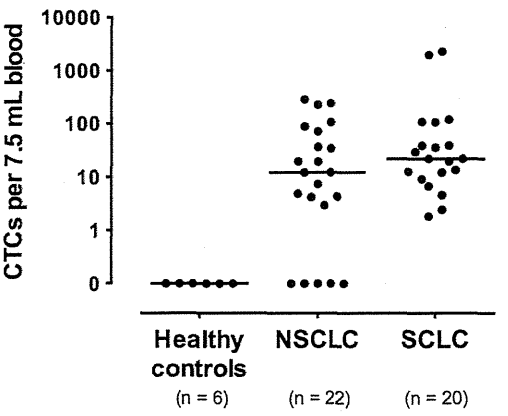


**Figure 2. CTC count using the MCA system.** CTC count/7.5 mL blood is shown for 6 healthy donors, 22 NSCLC patients and 20 SCLC patients.
doi:10.1371/journal.pone.0067466.g002

### CTC Enumeration using the CellSearch System and the MCA System

To conduct blind comparison of the detection sensitivity of the CellSearch and MCA systems, blood samples were collected from 22 metastatic NSCLC and 21 SCLC patients between April 2011 and February 2012 and analyzed for determination of the number of patients identified as CTC positive by each system (Table 2). Of these samples, 1 sample collected from 1 SCLC patient was not evaluated by the MCA system because an insufficient volume of blood had been collected for processing by both systems. As a result, 17 of the 22 (77%) NSCLC patients were identified as CTC positive using the MCA system but only 7 of the 22 (32%) NSCLC patients using the CellSearch system (Table 3). Of these patients, 8 were identified as CTC positive by both the CellSearch system

and the MCA system, 1 was identified as CTC positive by the CellSearch system only, and 9 were identified as CTC positive by the MCA system only. Considering the results obtained by both systems together, 18 (82%) of the NSCLC patients were identified as CTC positive. Analysis of these findings revealed that a significantly greater number of NSCLC patients were identified as CTC positive by the MCA system (median cell count 13, range 0–291 cells/7.5 mL; Figure 2) than by the CellSearch system (median cell count 0, range 0–37 cells/7.5 mL), demonstrating the statistical superiority of the MCA system in CTC enumeration ($p = 0.0015$, Wilcoxon test; Table 3).

In contrast, 20 of the 20 (100%) SCLC patients were identified as CTC positive using the MCA system versus 12 of the 21 (57%) patients using the CellSearch system. The median CTC count was found to be 2 cells/7.5 mL (range 0–325) using the CellSearch system and 23 cells/7.5 mL (range 2–2329) using the MCA system (Figure 2). Although not reaching a level of statistical significance, the detection sensitivity of the MCA system in CTC enumeration showed a trend toward being greater than that of the CellSearch system ($p = 0.2888$, Wilcoxon test; Table 3). For each outcome, agreement between the test results of the systems was assessed by Bland–Altman plots [33]. In the analysis of agreement regarding CTC enumeration in NSCLC patients, the mean difference was 50.1 (95% CI, range 11.1–89.1), with the limits of agreement ranging from −125.8 to 226.0. The MCA system yielded disproportionally higher CTC counts at higher mean values compared to The CellSearch system (Figure S2a). In contrast, in the analysis of agreement regarding CTC enumeration in SCLC patients, the mean difference was 202.6 (95% CI, range −116.7–521.9), with the limits of agreement ranging from −1162.0 to 1567.2. Unlike with the analysis of NSCLC blood samples, no bias was observed between the systems in the analysis of SCLC samples except for subjects with extremely high CTC titer (Figure S2b). Statistical analysis also revealed no association between site of metastasis and the CTC count of lung cancer patients using either system (data not shown).

**Table 2.** Patient characteristics.

| | | NSCLC | SCLC |
|---|---|---|---|
| **No. of patients** | | **22** | **21** |
| Gender | Male | 10 | 18 |
| | Female | 12 | 3 |
| Median age | | 68 | 73 |
| | (Range) | (36–77) | (53–83) |
| Smoking | Smoker | 16 | 21 |
| | Never-smoker | 6 | - |
| ECOG-PS | 0–1 | 16 | 13 |
| | 2–4 | 6 | 8 |
| No. of organs with metastasis | Median | 2 | 2 |
| | (Range) | (1–6) | (1–5) |
| Metastasis | Brain | 9 | 10 |
| | Bone | 8 | 4 |
| | Liver | 6 | 6 |
| Histology | Adenocarcinoma | 14 | – |
| | Squamous | 3 | – |
| | Others | 5 | – |
| | SCLC | – | 21 |

doi:10.1371/journal.pone.0067466.t002

**Table 3.** Comparison of CTC enumeration by the CellSearch system and the MCA system.

| Sample ID | | CellSearch CTC (cells/7.5 mL) | MCA CTC (cells/7.5 mL) |
|---|---|---|---|
| NSCLC | 1 | 0 | 0 |
| | 2 | 0 | 0 |
| | 3 | 9 | 0 |
| | 4 | 0 | 0 |
| | 5 | 0 | 5 |
| | 6 | 0 | 8 |
| | 7 | 2 | 90 |
| | 8 | 0 | 13 |
| | 9 | 0 | 13 |
| | 10 | 0 | 3 |
| | 11 | 1 | 35 |
| | 12 | 37 | 20 |
| | 13 | 2 | 246 |
| | 14 | 18 | 108 |
| | 15 | 0 | 73 |
| | 16 | 10 | 231 |
| | 17 | 19 | 20 |
| | 18 | 1 | 4 |
| | 19 | 0 | 0 |
| | 20 | 0 | 4 |
| | 21 | 0 | 291 |
| | 22 | 0 | 38 |
| SCLC | 23 | 200 | 20 |
| | 24 | 189 | 30 |
| | 25 | 0 | 13 |
| | 26 | 0 | 9 |
| | 27 | 0 | 40 |
| | 28 | 0 | 7 |
| | 29 | 33 | 23 |
| | 30 | 2 | 14 |
| | 31 | 3 | 122 |
| | 32 | 18 | 2 |
| | 33 | 1 | 2329 |
| | 34 | 1 | 2021 |
| | 35 | 4 | 13 |
| | 36 | 15 | 5 |
| | 37 | 325 | 40 |
| | 38 | 2 | – |
| | 39 | 13 | 36 |
| | 40 | 110 | 110 |
| | 41 | 0 | 3 |
| | 42 | 0 | 23 |
| | 43 | 0 | 109 |

doi:10.1371/journal.pone.0067466.t003